

Supporting Information

Singlet Fission in Core-Shell Micelles of End-Functionalized Polymers

Andrew J. Tilley,¹ Ryan D. Pensack,² Emily L. Kynaston,¹ Gregory D. Scholes,^{2,} and Dwight S. Seferos^{1,3*}*

*Correspondence to: dseferos@chem.utoronto.ca; gscholes@princeton.edu

¹Lash Miller Chemical Laboratories, Department of Chemistry, University of Toronto, 80 St. George Street, Toronto, ON M5S 3H6, Canada

²Department of Chemistry, Princeton University, Princeton, NJ 08544, USA

³Department of Chemical Engineering and Applied Chemistry, University of Toronto, 200 College Street, Toronto, Ontario M5S 3E5, Canada

Table of Contents

| | |
|--|----|
| Section S1: Experimental Methods | 3 |
| S1.1 – General methods and instrumentation | 3 |
| S1.2 – Dynamic light scattering | 3 |
| S1.3 – Steady state photophysics | 4 |
| S1.4 – Transient absorption spectroscopy | 4 |
| S1.5 – Time-correlated single photon counting (TCSPC) | 5 |
| S1.6 – Details of kinetics analysis | 6 |
| Section S2: Synthesis | 10 |
| S2.1 – Compound synthesis | 10 |
| S2.2 – Representative procedure for CuAAC ‘click’ reaction between 4 and azide-terminated PEG polymers | 14 |
| S2.3 – Synthesis of core-shell micelles of Pn-PEG and Pn-PEG-Pn | 14 |
| S2.4 – Representative procedure for the synthesis of mixed | |

| | |
|---|----|
| micelles – 10:1 C ₁₆ -PEG/Pn-PEG | 15 |
| S2.5 – Molecular structure of the C ₁₆ -PEG surfactant (polyethylene glycol hexadecyl ether, also known as Brij 58) (M _n ~1124 Da) | 15 |
| S2.6 – Estimation of the lengths of single Pn-PEG and Pn-PEG-Pn chains | 15 |
| Section S3: Micelle characterization and photophysical data | 16 |
| S3.1 – Additional evidence supporting polymer chain cyclization | 16 |
| S3.2 – Singlet fission in the micelles occurs exclusively at weakly excitonically coupled dimer pair sites | 16 |
| S3.3 – The role of pentyltriazole-PEG on singlet fission dynamics | 20 |
| S3.4 – Calculation of the total surface area:volume (SA:V) ratio of the micelle core | 21 |
| S3.5 – Evidence supporting C ₁₆ -PEG incorporation within the micelles | 22 |
| Section S4: NMR spectra | 48 |
| References | 54 |

Section S1: Experimental Methods

S1.1 - General methods and instrumentation

Dry THF was obtained from an Innovative Technology Pure Solv solvent purification system, and degassed by $3 \times$ freeze-pump-thaw cycles. Dichloromethane (DCM) and methanol were obtained from commercial suppliers and used as received. Thin layer chromatography was performed on aluminum plates pre-coated with Merck silica gel 60. Detection was achieved via irradiation by UV light. Column chromatography was performed using SiliaFlash silica gel (Silicycle Inc.) as the stationary phase and the column eluted using compressed air. Solvent mixtures used and their composition are indicated in the relevant procedure. All ^1H and ^{13}C NMR spectra were recorded on Varian Mercury 400, Bruker Avance III 400 or Agilent 500 instruments. Chemical shifts (δ) are expressed in parts per million (δ) using residual solvent (^1H NMR δ 7.26 ppm for CDCl_3 ; ^{13}C NMR δ 77.16 ppm for CDCl_3) as reference. High resolution mass spectra were recorded using a JEOL AccuTOF (DART) mass spectrometer. MALDI mass spectra were obtained using a Bruker Microflex MALDI-TOF mass spectrometer from a matrix of dithranol (2500:1 matrix-to-polymer ratio) cast from chloroform solution. Transmission Electron Microscopy (TEM) was performed on a Zeiss Leo 912B energy filtered TEM equipped with a LaB6 filament. All TEM images were collected in bright-field mode at an accelerating voltage of 120 kV. Samples were prepared by depositing $\sim 10 \mu\text{L}$ of the micelle suspension onto lacey carbon support film grids (400 mesh, Copper) purchased from Ted Pella, Inc (product #01824), followed by drying in the dark under ambient conditions for a minimum of 3 hours. (5-bromo-1-pentynyl)trimethylsilane (**2**) was synthesized according to a literature procedure.¹ 4-bromo-1,2-*bis*(dibromomethyl)benzene was purchased from AK Scientific, and used as received. Reagent-grade 1,4-dihydroxyanthraquinone, Tris[(1-benzyl-1H-1,2,3-triazol-4-yl)methyl]amine (TBTA), poly(ethylene glycol) bisazide ($M_n = 1100$ Da), poly(ethylene glycol) methyl ether azide ($M_n = 1000$ Da), and polyethylene glycol hexadecyl ether (Brij 58, $M_n \sim 1124$ Da) were purchased from Sigma-Aldrich and used as received. Number-average molecular weight values for PEG polymer precursors and Brij 58 are as-quoted from the supplier.

S1.2 - Dynamic light scattering

Dynamic light scattering measurements were performed on a Malvern Instruments Zetasizer Nano ZS instrument equipped with a Helium Neon laser ($\lambda = 633$ nm). All measurements were

performed in quartz cuvettes at 25 °C. Hydrodynamic diameters are quoted as the Z-average diameter, which is the intensity-weighted mean diameter of particles in the sample.

S1.3 – Steady state photophysics

Optical absorption spectra were recorded on a Varian Cary 5000 UV-Vis spectrophotometer. All solution absorption spectra were recorded against solvent blanks in matched 1.0 cm path length quartz cells. Fluorescence spectra were recorded on a Photon Technology International (PTI) QuantaMaster 40-F NA spectrofluorometer using a xenon arc light source and 914 Photomultiplier Detection System using spectroscopic grade solvents. The optical densities of the solutions were kept below 0.20 at the absorption maximum to minimize reabsorption effects.

S1.4 - Transient absorption spectroscopy

Transient absorption spectroscopy was performed using a setup described in detail previously.^{2,3} In brief, transient absorption measurements were performed with a 1 kHz regeneratively amplified Ti:sapphire laser system (Coherent Libra, Santa Clara, California) that provides ~50 fs pulses at ~800 nm with an average power of ~4 W. A beamsplitter at the output of the laser amplifier served to generate separate pump and probe beam paths. A large fraction of the power was used to drive an optical parametric amplifier (Light Conversion OPerA Solo, Vilnius, Lithuania) to convert the 800 nm radiation to ca. 650 nm, the latter being a pump wavelength suitable for resonant excitation. The pump and probe arms, with the latter comprising a small fraction of the power of the laser amplifier, were directed towards a commercial transient absorption spectrometer (Ultrafast Systems Helios, Sarasota, Florida). A mechanical delay stage, with optical elements designed specifically for 800 nm radiation, served to provide the pump and probe time delay; the 800 nm radiation in the probe arm was subsequently used to generate a continuum either in the visible (ca. 420 to 760 nm) or near-infrared (ca. 850 to 1600 nm) spectral region. Optical filters were used to isolate the continuum from the 800 nm radiation. The relative pump and probe polarization was controlled with a combination of a $\lambda/2$ waveplate and polarizer in the probe beam path situated before continuum generation. Measurements were performed with pump and probe polarizations oriented at the sample oriented at the magic angle with respect to one another.

The nanoparticle and micellar suspensions were contained in a 2 mm path length glass spectrophotometer cell (Starna Cells, Atascadero, California). The samples were stirred over the course of the measurements by placing a teflon-coated magnetic stir bar inside the sample cell, and by placing a magnet attached to a motor on the immediate exterior of the sample cell. Samples were prepared with an optical density at the excitation wavelength of ca. 0.40 or less.

The pump beam spot size was determined by placing a digital CCD camera (Thorlabs Inc., Newton, New Jersey) at focal plane of the probe in the region of pump and probe overlap and analyzing an image obtained using ThorCam software (Thorlabs Inc., Newton, New Jersey). The spot size determined in this manner was ca. 170 μm . An optical power sensor and meter (Coherent Inc., Santa Clara, California) was used to measure pulse energies. Typical incident pump fluences for measurements probing in the visible and near-infrared spectral region were ca. 130 and 260 $\mu\text{J}/\text{cm}^2$, respectively. The pump pulse duration of ca. 110 ± 5 fs measured at a similar wavelength of 710 nm has been reported previously.² Sample degradation was observed during the course of collecting the NIR transient absorption spectra (see Figure S5) of the neat micelles due to the long collection times required to obtain adequate signal-to-noise (~4 hours), possibly due to a photodimerization process. This is evidenced by clear bleaching of the visible ground state absorption band (Figure S5).

S1.5 – Time-correlated single photon counting (TCSPC)

Time-resolved fluorescence measurements were made using a DeltaFlex TCSPC spectrometer (HORIBA Scientific, Edison, NJ). The excitation and emission wavelengths were 507 and 650 nm, respectively. The optical density of the sample at the maximum of the lowest-energy electronic transition was ~0.4 or less which corresponded to an optical density of ~0.04 or less at the excitation wavelength. The sample was contained in a 1 cm fluorimeter cell (Starna Cells Inc, Atascadero, CA). The instrument response function was obtained by placing an aqueous Ludox colloidal silica suspension, which efficiently scatters the excitation light, into the spectrometer while keeping all settings equivalent to those used for the sample. The instrument response function exhibited a full-width at half maximum of ca. 200 ps, which is representative of the time resolution of the TCSPC spectrometer (Figure S20).

S1.6 - Details of kinetics analysis

TCSPC

TCSPC kinetics traces were fit according to a multi-exponential function with the following functional form:

$$I(t) = \sum_i A_i e^{t/\tau_i}$$

where the number of exponentials necessary to model the data was determined in a manner that will be described below. For the purpose of modeling the data, the multi-exponential fit function was also convolved with the instrument response function shown in Figure S20.

The number of exponentials necessary to model the data was determined by modeling the TCSPC kinetics with successively more exponentials and evaluating the resultant fit parameters, and also the residuals and Pearson's "exact" χ^2 values. The former were evaluated for physical reasonability whereas the latter were evaluated for improved quality of fit. In terms of the fit parameters and their physical reasonability, amplitudes that were negative or several orders-of-magnitude smaller than those determined for other fit parameters were considered physically unreasonable. Lifetimes beyond the ca. 40 ns natural lifetime of TIPS-Pn were considered physically unreasonable. In terms of metrics used to evaluate the quality of fit, residuals (i.e., the difference between the data and the fit) were used to compare additional structure in the fits that was accounted for with the inclusion of an additional exponential function in the fit. Pearson's "exact" χ^2 values were determined in a manner as outlined by Hall and Selinger, as follows:⁴

$$\sum \frac{(data - fit)^2}{fit}$$

If Pearson's "exact" χ^2 value did not change or became worse with the introduction of an additional exponential function in the fit, we considered the inclusion of an additional exponential function unnecessary. On a quantitative level, we found the inclusion of an additional exponential function to be justified when, prior to the inclusion of the additional exponential function, Pearson's "exact" χ^2 value was larger by a value of ca. 140% or more.

This statement was additionally verified by considering, as described above, the physical reasonability of the fit parameters along with the quality of the residuals.

Transient absorption spectroscopy

Because transient absorption spectroscopy simultaneously monitors both “bright”, emissive populations and “dark”, non-emissive populations (in the present context, parent singlet excitations and triplet pairs, respectively) and because the “dark”, non-emissive population of triplet pairs exhibits a lifetime dependent on excitonic coupling strength,⁵⁻⁷ a different means to model the data than that described above for the TCSPC traces was necessary.

To model the TA kinetics, the data were first obtained by averaging over a spectral range of 445 to 460 nm which is primarily associated with parent singlet excitations (although there is a small contribution in this region from triplet pairs and isolated-molecule triplet excitations). Thus, given that parent singlet excitons, triplet pairs, and isolated-molecule triplet excitations absorb in this spectral region, we can expect the signal to decay to some non-zero offset as parent singlet excitons convert to triplet pairs. This was accounted for by modeling the data in the following manner:

$$I(t) = \left(\sum_i A_i e^{t/\tau_i} \right) + B$$

where B is a value accounting for this non-zero offset.

While the introduction of an offset parameter into the fit was able to account for the different absorption strengths of the parent singlet and triplet pair populations, the latter population has been shown to be able to decay rapidly with a lifetime dependent on excitonic coupling strength.⁵⁻⁷ Although many attempts were made to develop a model to account for the subsequent decay of the triplet pair populations, we were unable to converge to a model that satisfactorily described the data for all samples, likely as a result of the complex distribution of environments and therefore triplet pair populations generated in these amorphous samples. In

order to circumvent these challenges yet still gain physical insight into the singlet fission dynamics, we limited our analysis to determining triplet pair formation time constants in the samples. This was accomplished by truncating the datasets to a timescale where the triplet pair population had reached its maximum amount. The timescale where the triplet pair population had reached its maximum amount was determined by considering the time at which the triplet pair transient absorption signal had reached its maximal value.

For the 0:1, 10:1, and 100:1 C₁₆-PEG:Pn-PEG samples, these values were 200 ps, 7.5 ns, and 7.5 ns, respectively. In other words, we found the triplet pair population to exhibit its maximal signal in the 0:1 C₁₆-PEG:Pn-PEG sample on a timescale of ca. 200 ps and in the 10:1 C₁₆-PEG:Pn-PEG sample on a timescale of ca. 7.5 ns. In the case of the 0:1 C₁₆-PEG:Pn-PEG sample where the triplet pair signal maximized at ca. 200 ps, the signal thereafter decayed which compromises the analysis of any longer triplet pair formation time constants (as determined via TCSPC measurements) because the decaying signal from the parent singlet exciton population overlaps the decaying signal of the triplet pair population. Such a physical scenario requires a more sophisticated kinetic model that we were unable to develop in the present work. As described in the main text, we found no evidence for singlet fission in the 100:1 C₁₆-PEG:Pn-PEG sample which justified modeling these data over the range of 7.5 ns, i.e., the entire range of the TA measurement. For the 10:1 C₁₆-PEG:Pn-PEG sample, the triplet pair signal maximized at ca. 7.5 ns which enabled us to model the triplet pair formation over the corresponding time range.

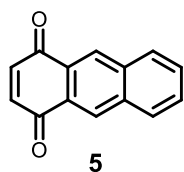
For the 0:1, 10:1, and 100:1 C₁₆-PEG:Pn-PEG-Pn samples, these values were 200 ps, 500 ps, and 7.5 ns, respectively. That is, we found the triplet pair signal to maximize at timescales of ca. 200 and 500 ps, respectively, for the 0:1 and 10:1 C₁₆-PEG:Pn-PEG-Pn samples, and truncated the datasets at these timescales to avoid biasing the fits to the decay of the parent singlet excitation population with the decay of the triplet pair population. Because singlet fission was not the predominant decay pathway in the 100:1 C₁₆-PEG:Pn-PEG-Pn sample, we were able to model the data over the entire time range of 7.5 ns.

In a manner similar to that described above, we found that a single-exponential function was sufficient to model the TA kinetics of the 0:1 and 100:1 C₁₆-PEG:Pn-PEG samples and 0:1 and

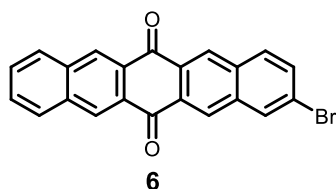
10:1 C₁₆-PEG:Pn-PEG-Pn samples in addition to the offset parameter, whereas two exponential functions were necessary to model the TA kinetics of the 10:1 C₁₆-PEG:Pn-PEG and 100:1 C₁₆-PEG:Pn-PEG-Pn samples in addition to an offset parameter. Given the especially good agreement between results of the TCSPC and TA kinetics analysis for the 100:1 C₁₆-PEG:Pn-PEG-Pn sample, we consider these results to justify a bi-exponential fitting for the sample for the two different measurement techniques. It should be noted that different time constants (and amplitudes) determined for the TCSPC and TA kinetics analysis for the 10:1 C₁₆-PEG:Pn-PEG sample arises due to the different time resolution of the different measurement techniques and also because of the limitations of modeling the TA kinetics as described above.

Section S2: Synthesis

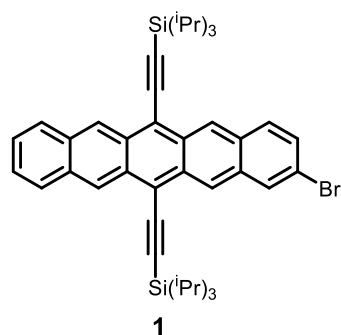
S2.1 – Compound synthesis



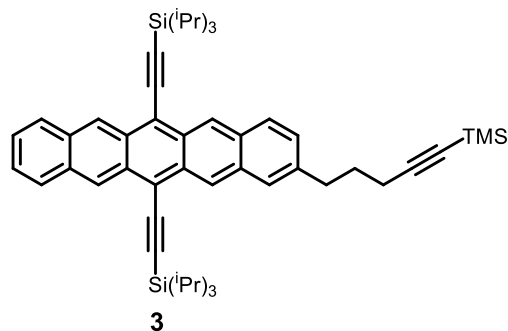
Following a reported procedure,⁸ sodium borohydride (0.949 g, 25.09 mmol) was added portionwise to a stirred solution of 1,4-dihydroxyanthraquinone (1.504 g, 6.26 mmol) in MeOH at 0 °C. Once the addition was complete, the reaction mixture was allowed to warm to room temperature, and stirred under argon for 15 h. After 15 h at room temperature, the reaction mixture was cooled to 0 °C and 20 mL of 6 M HCl added dropwise. The resultant orange solid was collected by vacuum filtration, and washed with H₂O (~50 mL). The filtrate was recovered in CHCl₃, dried (MgSO₄), filtered, and concentrated under reduced pressure to give the title compound as a bright orange solid that required no further purification (1.276 g, 98%). ¹H NMR (CDCl₃, 400 MHz) δ 7.06 (s, 2H), 7.67-7.72 (m, 2H), 8.03-8.09 (m, 2H), 8.61 (s, 2H). ¹³C NMR (CDCl₃, 500 MHz) δ 128.51, 129.00, 129.73, 130.36, 134.96, 140.19, 184.80.



Following a reported procedure,⁹ 4-bromo-1,2-bis(dibromomethyl)benzene (9.007 g, 17.99 mmol) and **5** (3.568 g, 17.14 mmol) were dried under high vacuum for one hour, then 110 mL of DMF added. The reaction mixture was stirred and heated under argon at 110 °C for 21 h. After 21 h, the reaction was allowed to cool to room temperature and poured into ~200 mL of rapidly stirring MeOH at 0 °C. The solid precipitate was collected by vacuum filtration and washed sequentially with MeOH, H₂O, and then again with MeOH (to remove excess H₂O), and finally a small volume of CHCl₃ to give the title compound as a light brown/tan solid (4.330 g, 65%). The product was found to be largely insoluble in common organic solvent, and so was not characterized by NMR spectroscopy. HRMS (DART⁺) *m/z* 387.0015 (C₂₂H₁₂BrO₂ [M+H]⁺ requires 387.0021).



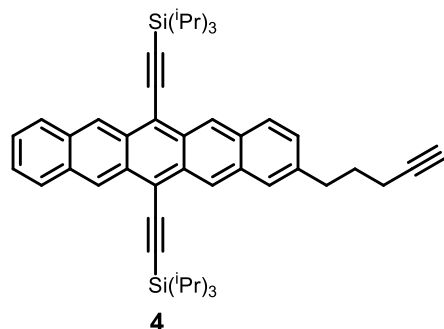
Following a reported procedure,⁵ *n*-butyl lithium (1.6 M, 1.6 mL, 2.560 mmol) was slowly added to a stirred solution of (triisopropylsilyl)acetylene (0.41 g, 0.50 mL, 2.25 mmol) in dry, degassed THF at -78 °C under argon. After stirring for 1 h at -78 °C, pentacene quinone **6** (0.250 g, 0.646 mmol) was added and the reaction mixture allowed to warm to room temperature, and stirred for 16 h. To the resultant deep yellow solution, 2.5 mL of a saturated solution of tin(II) chloride dihydrate in 10% HCl was added dropwise. The resultant deep blue reaction mixture was stirred for 1 h at room temperature, and then filtered over a short pad of silica (using DCM as eluent). The filtrate was collected and washed with H₂O (3 × 100 mL), and the combined aqueous fractions re-extracted with additional DCM (1 × 50 mL). The organic extracts were combined, dried (MgSO₄), filtered, and concentrated under reduced pressure to give a deep blue solid. The deep blue solid was purified by silica gel column chromatography using 100% hexanes as eluent to give the title compound as a deep blue solid (0.259 g, 56%). ¹H NMR (CDCl₃, 400 MHz) δ 1.35-1.44 (m, 42H), 7.40-7.46 (m, 3H), 7.84 (d, *J* 9.1 Hz, 1H), 7.95-8.00 (m, 2H), 8.13 (s, 1H), 9.19 (s, 1H), 9.27 (s, 1H), 9.30 (d, *J* 5.5 Hz, 2H). ¹³C NMR (CDCl₃, 500 MHz) δ 11.83, 19.15, 19.17, 104.53, 104.59, 107.72, 107.81, 118.65, 118.81, 120.45, 125.62, 126.34, 126.37, 126.51, 126.55, 127.08, 128.82, 129.69, 130.33, 130.38, 130.57, 130.69, 130.81, 130.96, 131.04, 132.55, 132.64, 132.77.



Preparation of Grignard reagent: Magnesium turnings (0.143 g, 5.865 mmol) were stirred in a flame-dried 3-neck flask under high vacuum overnight. Dry, degassed THF (6 mL) was added to the magnesium turnings, followed by a scoopula tip of iodine. Once the magnesium turnings were activated (as indicated by disappearance of the yellow colour), 0.5 mL of a solution of (5-bromo-1-pentynyl)trimethylsilane (1.292 g, 5.894 mmol) in dry, degassed THF (4 mL) was added and the reaction mixture heated to reflux for 5 mins using a heat gun. After 5 mins, the remaining 3.5 mL of the alkyl bromide solution was added over a period of 15 minutes, and the resultant brown solution heated at reflux for 4 h to give a final concentration of Grignard reagent of 0.37 M. The Grignard reagent was then used immediately in the next step.

Kumada coupling: **1** (1.097 g, 1.528 mmol) was taken up in 15 mL of dry, degassed THF and added to a flame-dried flask containing Pd(dppf)Cl₂.DCM (0.125 g, 0.153 mmol). Grignard reagent **2** (0.37 M, 6.200 mL, 2.294 mmol) was then added over a period of ~5 minutes and the reaction mixture stirred at room temperature in the dark for 16 h. The reaction was quenched by adding 20 mL of sat. aq. NaHCO₃, and then diluted with DCM (200 mL). The organic layer was washed with sat. aq. NaHCO₃ (2 × 150 mL), sat. aq. NaCl (2 × 150 mL), and the combined aqueous layers re-extracted with additional DCM (2 × 50 mL). The organic extracts were combined, dried (MgSO₄), filtered, and concentrated under reduced pressure to give a deep blue waxy solid. Purification of the crude product by silica gel column chromatography (gradient of 0-5% DCM/hexanes as eluent) afforded the title compound as a deep blue solid (0.799 g, 67%). ¹H NMR (CDCl₃, 400 MHz) δ 0.20 (s, 9H), 1.35-1.46 (m, 42H), 1.94-2.04 (m, 2H), 2.34 (t, *J* 6.97 Hz, 2H), 2.92 (t, *J* 7.5 Hz, 2H), 7.27-7.30 (m, 1H), 7.38-7.43 (m, 2H), 7.70 (s, 1H), 7.91 (d, *J* 8.8 Hz, 1H), 7.94-8.00 (m, 2H), 9.20 (s, 1H), 9.26 (s, 1H), 9.29 (m, 2H). ¹³C NMR (CDCl₃, 400 MHz) δ 0.37, 11.84, 19.15, 19.18, 19.19, 19.21, 19.53, 19.95, 28.38, 28.61, 29.72, 35.30, 77.36, 85.36, 104.89, 104.92, 107.12, 107.14, 118.22, 118.49, 125.42, 126.07, 126.11, 126.18, 126.40,

126.42, 126.49, 128.33, 128.81, 128.94, 130.61, 130.62, 130.82, 130.95, 131.55, 132.31, 132.39, 132.63, 139.42. HRMS (DART⁺) *m/z*. 777.4701 (C₅₂H₆₉Si₃ [M+H]⁺ requires 777.4707).



K₂CO₃ (0.778 g, 5.629 mmol) was added to a stirred solution of **3** (0.290 g, 0.373 mmol) in DCM/MeOH (20 mL, 1:3 v/v) at room temperature, and the reaction mixture heated at reflux for 16 h. The reaction mixture was diluted with additional DCM (100 mL) and washed with sat. aq. NaHCO₃ (3 × 100 mL). The aqueous layers were re-extracted with additional DCM (1 × 50 mL), and the combined organic extracts dried (MgSO₄), filtered, and concentrated under reduced pressure to give a deep blue solid. Purification of the crude product by silica gel column chromatography (gradient of 0-10% DCM/hexanes as eluent) afforded the title compound as a deep blue solid (0.189 g, 72%). ¹H NMR (CDCl₃, 500 MHz) δ 1.35-1.47 (m, 42H), 1.97-2.04 (m, 2H), 2.06 (t, *J* 2.6 Hz, 1H), 2.29-2.34 (m, 2H), 2.95 (t, *J* 7.5 Hz, 2H), 7.29 (dd, *J* 8.9 Hz, *J* 1.1 Hz, 1H), 7.39-7.44 (m, 2H), 7.73 (s, 1H), 7.92 (d, *J* 8.8 Hz, 1H), 7.95-8.05 (m, 2H), 9.21 (s, 1H), 9.27 (s, 1H), 9.30 (s, 2H). ¹³C NMR (CDCl₃, 500 MHz) δ 11.84, 11.85, 18.09, 19.15, 19.18, 29.44, 35.20, 69.03, 76.84, 77.16, 77.48, 84.25, 104.88, 104.91, 107.14, 107.15, 118.24, 118.49, 125.47, 126.08, 126.11, 126.18, 126.40, 126.43, 126.53, 128.30, 128.81, 128.97, 130.61, 130.63, 130.81, 130.96, 131.54, 132.32, 132.39, 132.60, 139.21. HRMS (DART⁺) *m/z* 705.4298 (C₄₉H₆₁Si₂ [M+H]⁺ requires 705.4312).

S2.2 - Representative procedure for CuAAC 'click' reaction between **4** and azide-terminated PEG polymers

Into a 20 mL scintillation vial was placed $[\text{Cu}(\text{CH}_3\text{CN})_4][\text{PF}_6]$ (0.0085 g, 0.023 mmol) and TBTA (0.027 g, 0.051 mmol). Dry, degassed THF (5 mL) was added and the resultant solution allowed to stir at room temperature under argon for 1 h to ensure quantitative complexation. The copper-ligand complex solution was then added to a stirred solution of diazide-PEG ($M_n = 1100$ Da, 0.0261 g, 0.024 mmol) and TIPS-Pn-alkyne **4** (0.097 g, 0.138 mmol) in 5 mL of dry, degassed THF solution at room temperature under argon. *N,N*-diisopropylethylamine (1 drop, $\sim 10 \mu\text{L}$) was then added to the reaction mixture, and the deep blue solution stirred at room temperature under argon for 48 h. The reaction mixture was diluted with DCM (50 mL) and washed with sat. aq. NaHCO_3 (3×100 mL), dried (MgSO_4), filtered, and concentrated under reduced pressure to give a deep blue waxy solid. Purification of the crude product by silica gel column chromatography (100% DCM to elute excess **4**, followed by a gradient of 2-8% MeOH/ CHCl_3 to elute the product fraction) afforded the title compound as a deep blue solid (0.0418 g, 70%). ^1H NMR (CDCl_3 , 400 MHz) δ 1.33-1.43 (m, 84H), 2.12-2.22 (m, 4H), 2.82-2.93 (m, 8H), 3.50-3.67 (m, $(\text{OCH}_2\text{CH}_2)_n$), 3.85 (t, J 5.2 Hz, 4H), 4.51 (t, J 5.2 Hz, 4H), 7.30 (m, 2H), 7.38-7.43 (m, 4H), 7.49 (s, 2H), 7.70 (s, 2H), 7.90 (d, J 9.0 Hz, 2H), 7.93-8.00 (m, 4H), 9.18 (s, 2H), 9.25 (s, 2H), 9.29 (m, 4H). MALDI-MS $M_n = 2360$ Da.

Following a similar procedure to that described above, Pn-PEG was obtained as a deep blue solid after 50 h at room temperature (0.020 g, 51%). ^1H NMR (CDCl_3 , 400 MHz) δ 1.34-1.41 (m, 42H), 2.11-2.22 (m, 2H), 2.82-2.92 (m, 4H), 3.37 (s, 3H), 3.57-3.66 (m, $(\text{OCH}_2\text{CH}_2)_n$), 3.85 (t, J 5.3 Hz, 2H), 4.51 (t, J 5.1 Hz, 2H), 7.28 (m, 1H), 7.37-7.43 (m, 2H), 7.49 (s, 1H), 7.70 (s, 1H), 7.90 (d, J 9.0 Hz, 1H), 7.93-7.99 (m, 2H), 9.18 (s, 1H), 9.25 (s, 1H), 9.29 (m, 2H). MALDI-MS $M_n = 1870$ Da.

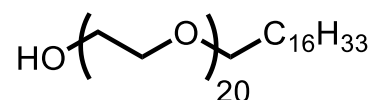
S2.3 - Synthesis of core-shell micelles of Pn-PEG and Pn-PEG-Pn

200 μL of an 800 μM solution of polymer in THF was rapidly injected into 10 mL of vigorously stirring deionized water at room temperature, leading to spontaneous formation of core-shell micelles. The solutions were characterized by optical absorption spectroscopy, dynamic light scattering, and transmission electron microscopy, and used within 3-4 days of preparation.

S2.4 - Representative procedure for the synthesis of mixed micelles – 10:1 C₁₆-PEG/Pn-PEG

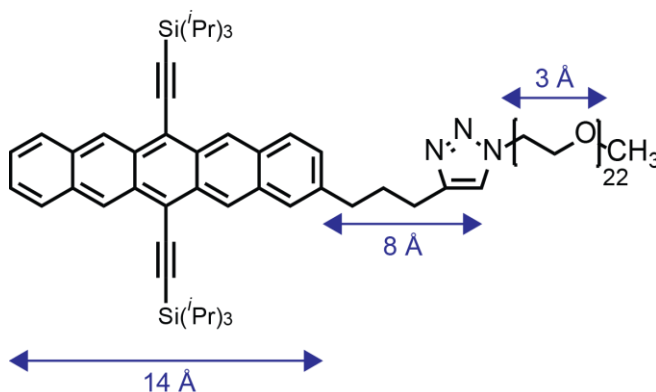
500 μL of an 800 μM solution of Pn-PEG in THF was prepared. A 10-fold molar excess of C₁₆-PEG surfactant (polyethylene glycol hexadecyl ether, $M_n \sim 1124$ Da) was added, and the resultant solution stirred for 1-2 minutes to ensure complete mixing. 200 μL of this solution was then rapidly injected into 10 mL of vigorously stirring water at room temperature, leading to spontaneous formation of mixed micelles. The solutions were characterized by optical absorption spectroscopy and dynamic light scattering, and used within 3-4 days of preparation.

S2.5 - Molecular structure of the C₁₆-PEG surfactant (polyethylene glycol hexadecyl ether, also known as Brij 58) ($M_n \sim 1124$ Da)



S2.6 – Estimation of the length of a single Pn-PEG chain

A chain length of ~ 8.8 nm for a single Pn-PEG polymer chain was estimated as follows. Firstly, we calculated the TIPS-Pn head-group to have an end-to-end length of ~ 22 Å. This was done by taking the pentacene end-to-end length as ~ 14 Å,¹⁰ and using an alkyl spacer length of ~ 8 Å (based on standard C-C bond lengths of ~ 1.5 Å) (see diagram below). The PEG chain has a number-average molecular weight (M_n) of ~ 1000 Da (corresponding to ~ 22 repeat units), and a repeat unit length of ~ 3 Å. Therefore, the polymer chain length can be approximated to be $14 + 8 + (3 \times 22)$ Å in length, which is equal to 8.8 nm. Using a similar strategy, the chain length of Pn-PEG-Pn is estimated to be ~ 10.7 nm.



Section S3: Micelle characterization and photophysical data

S3.1 – Additional evidence supporting polymer chain cyclization

Further evidence for polymer chain cyclization in Pn-PEG-Pn comes from considering the thermodynamics associated with polymer chain folding. In the case of Pn-PEG-Pn, the strong hydrophobic attraction of closely spaced TIPS-Pn end-groups is expected to create a thermodynamic driving force for cyclization strong enough to overcome the entropic loss associated with chain folding.¹¹ This expectation is supported by detailed experimental and theoretical work on the cyclization dynamics of telechelic PEG polymers end-capped with hydrophobic pyrene chromophores.^{12,13} A key finding of this work was that as the number-average molecular weight of the PEG decreased to ~4800 Da, the contribution of intrachain excimer emission increased due to the increasing hydrophobic attraction between pyrene units in aqueous solution driven by its strong exponential distance dependence.¹⁴ The hydrophobic interaction between terminal TIPS-Pn groups is expected to be even stronger in Pn-PEG-Pn due to the shorter chain length ($M_n \sim 1100$ Da), leading to immediate and irreversible polymer chain cyclization.

S3.2 - Singlet fission in the micelles occurs exclusively at weakly excitonically coupled dimer pair sites

Here, we show that singlet fission in the Pn-PEG and Pn-PEG-Pn micelles occurs exclusively at dimer pair sites comprising weakly excitonically coupled chromophores.

First, we discuss various physical processes contributing to the formation of triplet pairs in the Pn-PEG and Pn-PEG-Pn micelles. We previously showed that triplet pair formation in amorphous-phase samples can occur through a distribution of molecular packing arrangements with varying energetics and degrees of electronic coupling, through multiple phases of triplet pair formation including energy-migration limited singlet fission, or through a combination of these two distinct processes.^{15,16} As is argued in the main text, it is likely that some combination of these processes is responsible for the observed triplet pair formation dynamics in the Pn-PEG and Pn-PEG-Pn micelles.

We next focus the discussion on the nature of the dimer pair sites responsible for the formation of triplet pairs in the Pn-PEG and Pn-PEG-Pn micelles. In a pioneering work reporting super-unity triplet quantum yields in an amorphous film of a tetracene derivative, it was hypothesized that triplet pairs formed at dimer pair sites where the molecules adopt the equilibrium molecular packing of the single crystal.¹⁷ We previously showed that triplet pairs in amorphous TIPS-Pn nanoparticles, however, form largely at dimer pair sites where chromophores are weakly excitonically coupled, i.e., where the molecules do not adopt the equilibrium molecular packing of the single crystal.^{2,15,16} We show for the Pn-PEG and Pn-PEG-Pn micelles studied here that at no point over the course of the transient measurement is there evidence that triplet pairs form at dimer pair sites comprising strongly excitonically coupling chromophores; that is, triplet pair formation in the Pn-PEG and Pn-PEG-Pn micelles occurs exclusively at dimer pair sites comprising weakly excitonically coupled chromophores.

The first evidence indicating triplet pairs in the Pn-PEG and Pn-PEG-Pn micelles form exclusively at dimer pair sites comprising weakly excitonically coupled chromophores is shown in Figure SX1, which plots the 300 fs transient absorption spectra obtained from the Pn-PEG and Pn-PEG-Pn micelles along with the transient absorption spectrum of isolated-chromophore singlet excitations obtained from a dilute solution of TIPS-Pn in toluene.

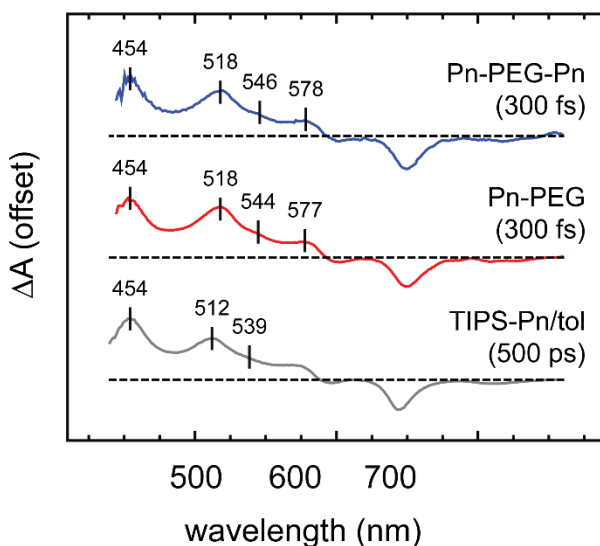


Figure S3.2.1. Transient absorption spectra of the Pn-PEG and Pn-PEG-Pn micelles obtained at a time delay of 300 fs plotted along with the transient absorption spectrum of isolated-chromophore singlet excitations obtained from a dilute solution of TIPS-Pn in toluene at a time delay of 500 ps.

Figure S3.2.1 shows that, although there are subtle redshifts of several bands of the vibronic progression in the micellar transient absorption spectra, the early-time transient absorption spectra of the micellar systems are nearly equivalent to that of the transient absorption spectrum of isolated chromophore singlet photoexcitations. The subtle redshifts likely arise from changes in the overlapping ground-state absorption spectrum which is modified by weak excitonic coupling (see main text). It is critical to note that the vibronic band of the singlet photoinduced absorption peaking at ca. 518 nm should not be confused with the origin vibronic band of the equilibrium-packing crystalline triplet photoinduced absorption that peaks at ca. 522 nm (see below). That is, although there is a photoinduced absorption band at early time in the transient spectra of the micellar systems, this arises from the singlet photoinduced absorption and not from a crystalline triplet photoinduced absorption.

We next compare the transient absorption spectra of the Pn-PEG and Pn-PEG-Pn micelles obtained at a time delay after singlet fission has been able to occur completely with the transient absorption spectra of triplets photogenerated on isolated molecules and in crystalline material (Figure S3.2.2).

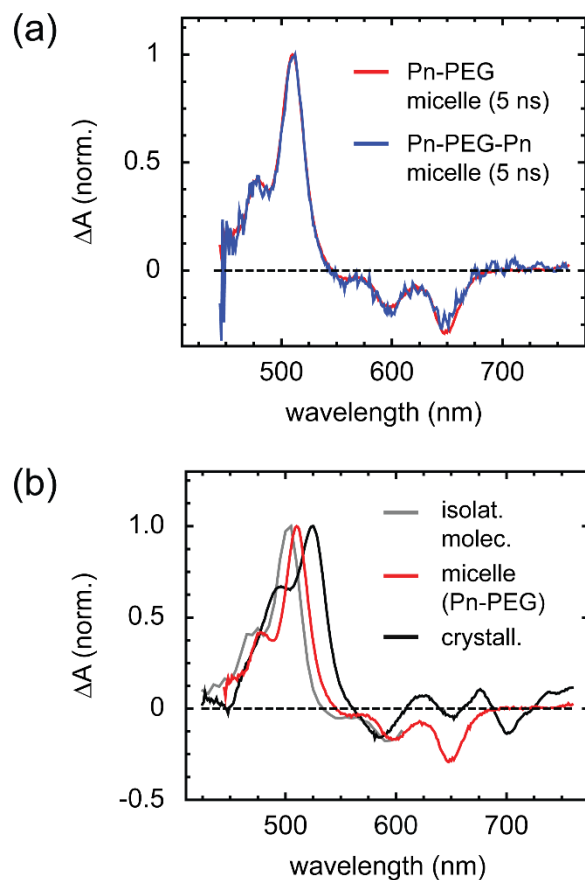


Figure S3.2.2. (a) Transient absorption spectra of the Pn-PEG and Pn-PEG-Pn micelles obtained at a time delay of 5 ns. (b) Transient absorption spectrum of the Pn-PEG micelles obtained at a time delay of 5 ns compared with transient absorption spectra of triplets photogenerated on isolated molecules and in crystalline (specifically, equilibrium-packing) material.

In Figure S3.2.2a, we first compare the transient absorption spectra of the Pn-PEG and Pn-PEG-Pn micelles obtained at a time delay of 5 ns. The spectra are nearly indistinguishable, with considerable noise apparent in the Pn-PEG-Pn spectrum. We therefore take the transient absorption spectrum of Pn-PEG micelles as representative of both material systems, and focus all subsequent discussion on this spectrum. Figure S3.2.2b shows the transient absorption spectrum of the Pn-PEG micelles compared with the transient absorption spectra of triplets photogenerated on isolated molecules and in crystalline material. Clearly, the transient absorption spectrum of the micelles better matches that triplets photogenerated on the isolated molecules. Specifically,

while there is a slight redshift of the vibronic progression in the triplets photogenerated in the Pn-PEG micelles (i.e., the origin band peaks at ca. 505, 510, and 524 nm for the isolated molecule, Pn-PEG micelle, and crystalline triplets, respectively), the vibronic progression (i.e., relative amplitudes) and linewidths more closely resemble that of triplets photogenerated on isolated molecules. Additionally, the transient absorption spectrum of the triplets photogenerated on crystalline material exhibit a prominent bleach feature at ca. 700 nm that is completely absent in the transient absorption spectrum of the Pn-PEG micelles. We can therefore rule out any contributions of singlet fission in the micelles from dimer pair sites comprising strongly excitonically coupled chromophores both via the lack of a redshifted absorption band in the ground-state absorption spectrum (see main text) and also via the fact that there are no features in the transient absorption spectrum of the micelles that match that of the equilibrium-packing crystalline material. We note that the two measurement techniques, i.e., steady-state and transient absorption, have sensitivities of the order of ca. 10^{-3} and 10^{-5} , respectively, which are sufficient to evaluate whether or not a minority population of dimer pair sites comprising strongly excitonically coupled chromophores contributes to these signals.

On the basis of the results reported above, we conclude that singlet fission in the micelles (and amorphous material more generally)^{2,15,16} occurs exclusively at dimer pair sites comprising weakly coupled chromophores.

S3.3 – The role of pentyltriazole-PEG on singlet fission dynamics

To investigate the effect of pentyltriazole-PEG on triplet pair formation dynamics in the micelles, we first precipitated nanoparticles of TIPS-Pn alkyne **4** and measured the triplet pair formation time using transient absorption spectroscopy. We hypothesized that the hydrophobic pentyltriazole linker would associate within the hydrophobic TIPS-Pn core, and therefore this control experiment would allow us to isolate the effect of this short hydrocarbon linker on triplet pair formation dynamics. The transient absorption spectrum of nanoparticles of **4** is consistent with singlet fission depleting the parent singlet exciton population (Figure S7). Using a similar kinetic analysis as for the micelle transient absorption data, we extracted a time constant for triplet pair formation in nanoparticles of **4** of ~ 7 ps. This is approximately one order of magnitude larger than the triplet pair formation time in nanoparticles of TIPS-Pn,^{2,15} and clearly

suggests that the linker is influencing the photophysics, presumably by frustrating intermolecular contacts between TIPS-Pn chromophores within the core.

The time constant for triplet pair formation in nanoparticles of **4** can be compared with the triplet pair formation time of ~30 ps measured for the star-like and flower-like micelles. While of a similar order of magnitude, the four-fold slower triplet pair formation time in the micelles suggests that the solubilizing PEG chains may also be affecting triplet pair formation dynamics. Given that the diameter of the micellar core constitutes ~75% of the total micelle diameter (based on the bright-field TEM images in Figure 1c), it is likely that the core contains a proportion of kinetically trapped PEG that disrupts TIPS-Pn π - π interactions and that may further contribute to the slower triplet pair formation time compared with solution nanoparticles of TIPS-Pn. It must be noted that dielectric screening of the TIPS-Pn core by the PEG corona is expected to make a negligible contribution to the reduced triplet pair formation time in the micelles (compared with TIPS-Pn solution nanoparticles), since >85% of TIPS-Pn chromophores are not in direct contact with the PEG corona (based on an estimate of the total surface area to volume ratio of the micelle core; see Section S3.4). Furthermore, it has been shown that amorphous nanoparticle suspensions of TIPS-Pn, which have an appreciable contact with water, exhibit essentially equivalent photophysics to amorphous films² thus ruling out water as having any influence on the photophysics.

S3.4 - Calculation of the total surface area:volume (SA:V) ratio of the micelle core

The bright-field TEM micrographs presented in Figure 1c of the main text were used to measure the size of the micellar cores. For this calculation we assume that the micelles are spherical, and use the standard equations for volume ($V = (4/3)\pi r^3$) and total surface area ($SA = 4\pi r^2$) of a sphere. It must be noted that the size of the cores when the micelles are dispersed in the aqueous media are almost certainly larger than what is determined by TEM due to the presence of kinetically trapped solvent molecules within the micelles that swell the solution structure. These molecules are removed during drying of the micelle samples for TEM and under the high vacuum conditions under which the sample is visualized. We therefore consider these calculated values to be an upper bound of the SA:V ratio of the micelle cores.

As seen in Table S1, the Pn-PEG micelles have a SA:V ratio of 0.125, and the Pn-PEG-Pn micelles have a SA:V ratio of 0.150. This implies that the proportion of TIPS-Pn chromophores directly interfaced with the PEG corona is, at most, 12.5% and 15.0% of the total population of chromophores. Thus, the majority of TIPS-Pn chromophores in the micelles occupy an environment similar to the environment experienced by TIPS-Pn chromophores in the solution aggregates studied in previous work,¹⁵ where triplet pairs form at a rate approximately one order of magnitude faster than in the micelles. We thus conclude that dielectric screening of the TIPS-Pn rich core by the PEG corona has a minimal influence on the observed order of magnitude reduction in triplet pair formation time.

Table S1: Geometric parameters of Pn-PEG and Pn-PEG-Pn micelle cores, as determined by TEM. A spherical geometry is assumed for calculation of core volume and core total surface area.

| Polymer | Core diameter (nm) | Core total surface area (nm ²) | Core volume (nm ³) | SA:V (nm ⁻¹) |
|-----------|--------------------|--|--------------------------------|--------------------------|
| Pn-PEG | 48 | 7238 | 57906 | 0.125 |
| Pn-PEG-Pn | 40 | 5027 | 33510 | 0.150 |

S3.5 – Evidence supporting C₁₆-PEG incorporation within the mixed micelles

Hydrodynamic diameters of control solutions of C₁₆-PEG precipitated at the same concentration used for precipitating the mixed micelles were recorded (Figure S12). These measurements show that C₁₆-PEG forms micelles at the same concentrations used in the 10:1 and 100:1 mixed micelle precipitation solutions, with Z-average hydrodynamic diameters of 9.66 and 9.49 nm. The absence of <10 nm particles in the mixed micelle suspensions (as determined by DLS) together with the increase in hydrodynamic diameter with increasing C₁₆-PEG:polymer ratio provides strong evidence of C₁₆-PEG incorporation within the micelles. We must note that we are unable to rule out the presence of a unimer population of solubilized C₁₆-PEG chains within the micelle suspensions using DLS. In fact, it is likely that the mixed micelles are composed of different relative molar quantities of C₁₆-PEG and polymer, and so we take the quoted ratio as representing the peak of the distribution of C₁₆-PEG:polymer incorporation ratios for the sample.

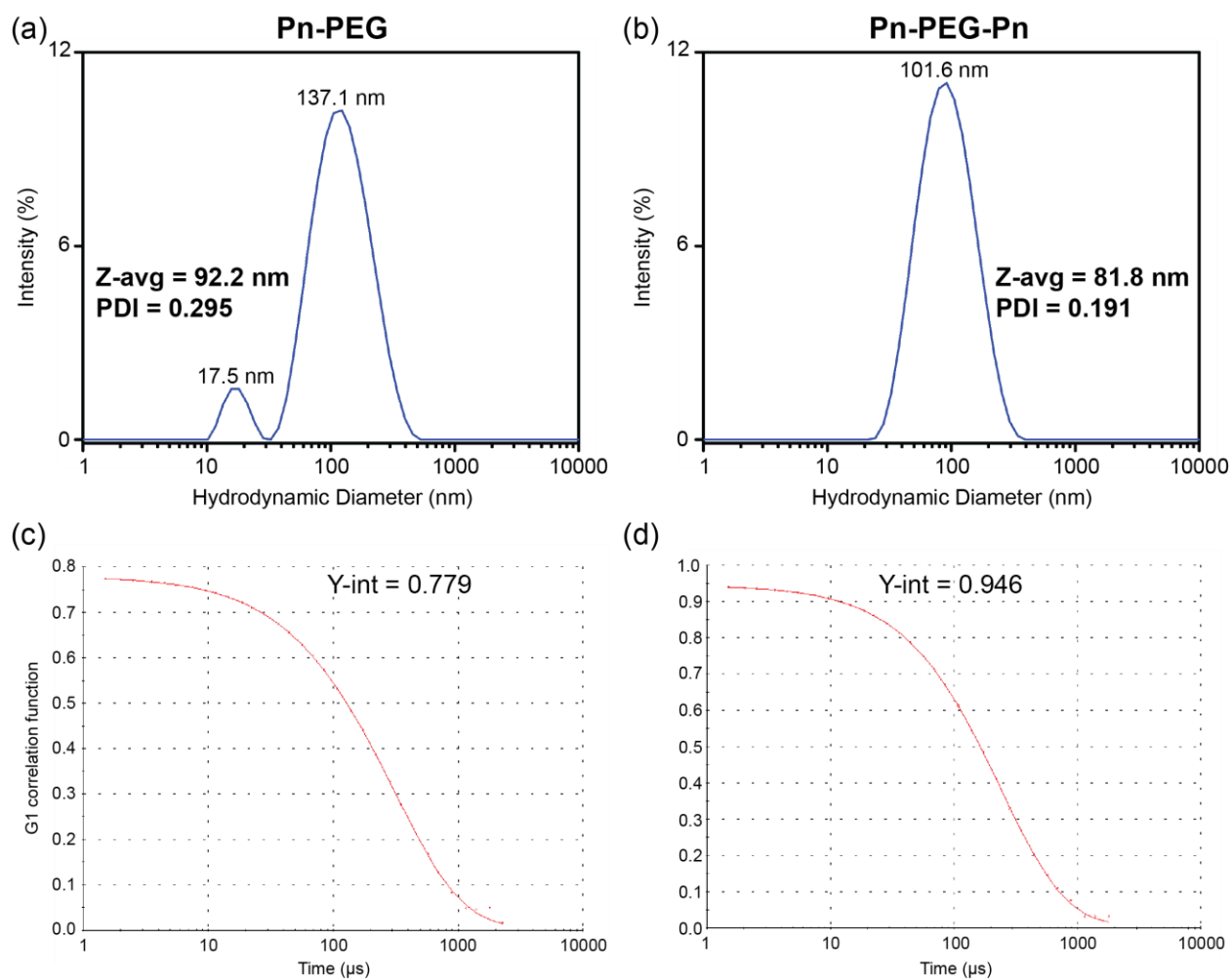


Figure S1: Results of dynamic light scattering experiments on aqueous suspensions of Pn-PEG and Pn-PEG-Pn micelles at 25 °C. Size distributions are shown in panels (a) and (b). Panels (c) and (d) show the autocorrelation functions used to extract particle size. Peak diameters are indicated next to the corresponding peak. PDI (polydispersity index) quantifies the dispersity of the sample, with values greater than 0.7 indicating a very polydisperse sample. The y-intercept (Y-int) indicates how well the autocorrelation function fits the data, with an ideal fit having Y-int = 1.

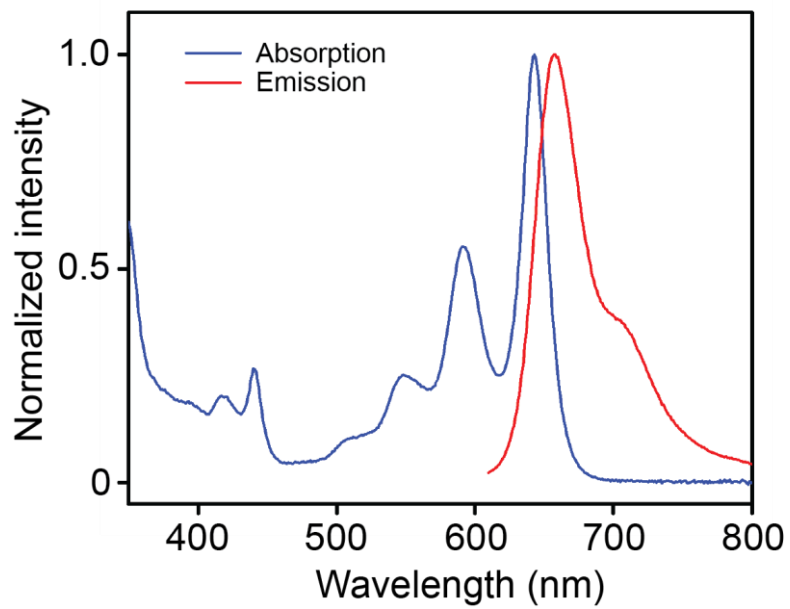


Figure S2: Optical absorption and emission spectra of Pn-PEG-Pn in dilute THF solution at room temperature.

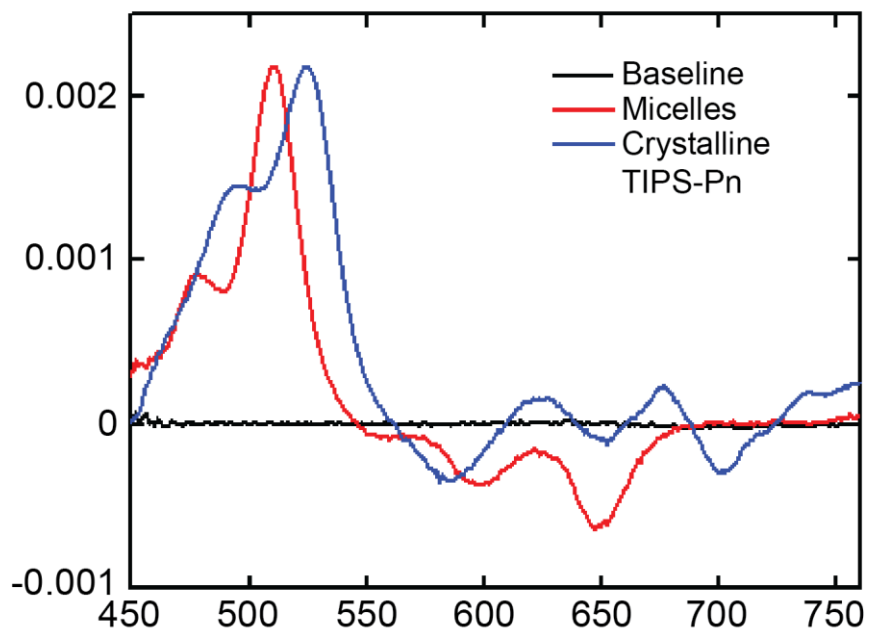


Figure S3: Transient absorption spectra of a negative time (-3 ps) baseline measurement demonstrating the 10^{-5} sensitivity of the TA measurement, of triplets photogenerated in the micelle (measured at 5 ns), and of triplets photogenerated in crystalline TIPS-Pn (measured at 1 ns). The response in the micelles is dominated by triplets that cannot be assigned to crystalline triplets.

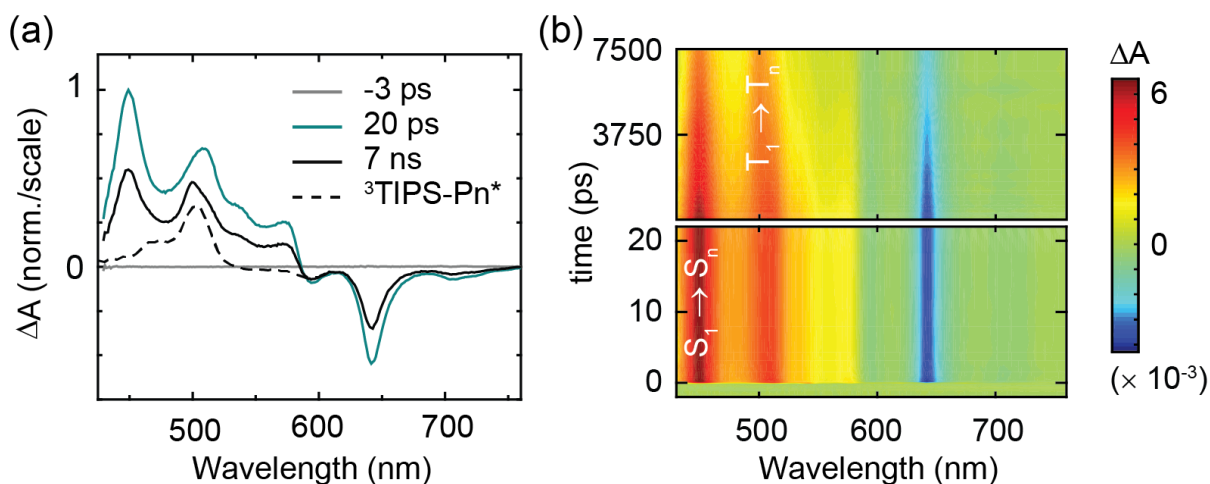


Figure S4: Transient absorption spectrum (panel (a)) of TIPS-Pn in dilute THF solution at room temperature. A pump wavelength of 647 nm was used. A triplet photoinduced absorption can be seen growing in over the nanosecond timescale (panel (b)), attributed to slow intersystem crossing.¹⁸ The triplet photoinduced absorption spectrum of TIPS-Pn is that of ³TIPS-Pn* in toluene as reported in R. D. Pensack, C. Grieco, *et al.*, *Mater. Horiz.* **4**, 915–923 (2017). The slight discrepancy in the peak position of the origin band of the triplet photoinduced absorption for TIPS-Pn in THF and TIPS-Pn in toluene likely arises from a solvatochromatic effect, which is also evident in the ground-state (S_0 - S_1) absorption. See eg. R. D. Pensack, A. J. Tilley, *et al.*, *J. Am. Chem. Soc.* **137**, 6790–6803 (2015).

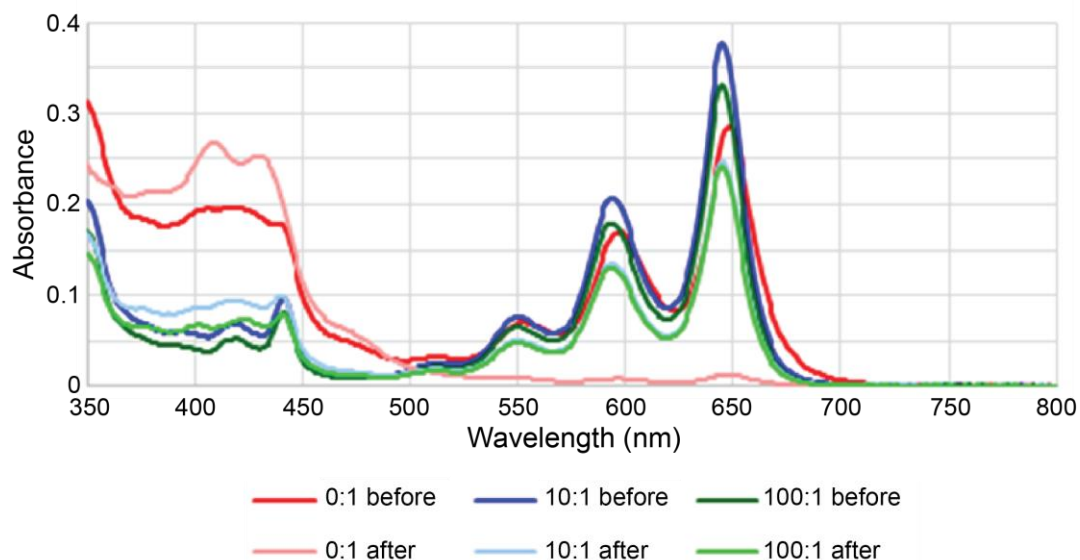


Figure S5: Optical absorption spectra of Pn-PEG micelles recorded before and after recording the NIR transient absorption spectra. The ratio indicated in the legend is the molar ratio of C₁₆-PEG:Pn-PEG in mixed micelles. Clear photobleaching of the visible absorption band (~500-670 nm) is observed for the ‘neat’ (0:1) micelles during the considerably long time required to collect the NIR transient absorption spectra (~4 hours), possibly due to a photodimerization process. By comparison, the mixed micelles are considerably more stable over the course of the experiment, presumably due to the ability of PEG to frustrate geometries favourable for photodimerization. To ensure consistency, we relied upon the visible transient absorption data to model the excited state dynamics of each sample studied in this work.

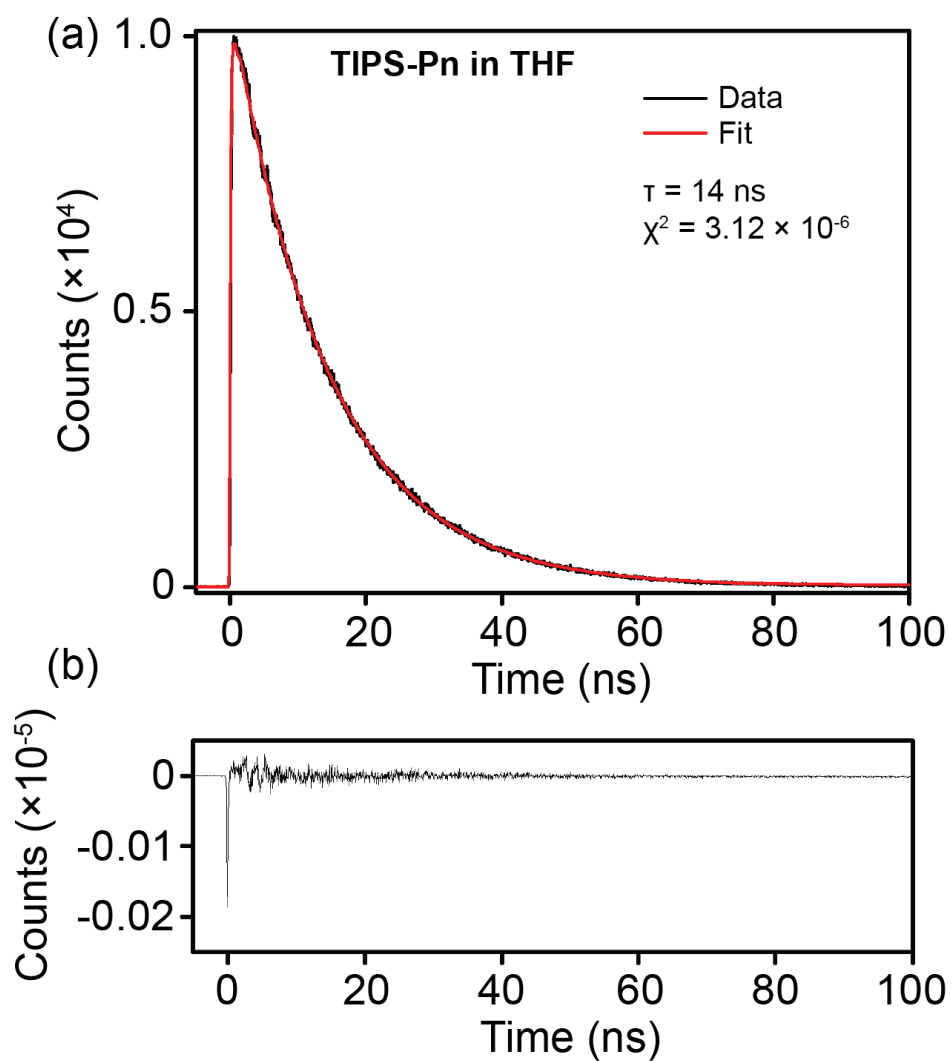


Figure S6: Fluorescence decay of a dilute solution of TIPS-Pn in deoxygenated THF (panel (a)). The residuals are shown in panel (b). The sample was excited at 570 nm and the emission monitored at 650 nm.

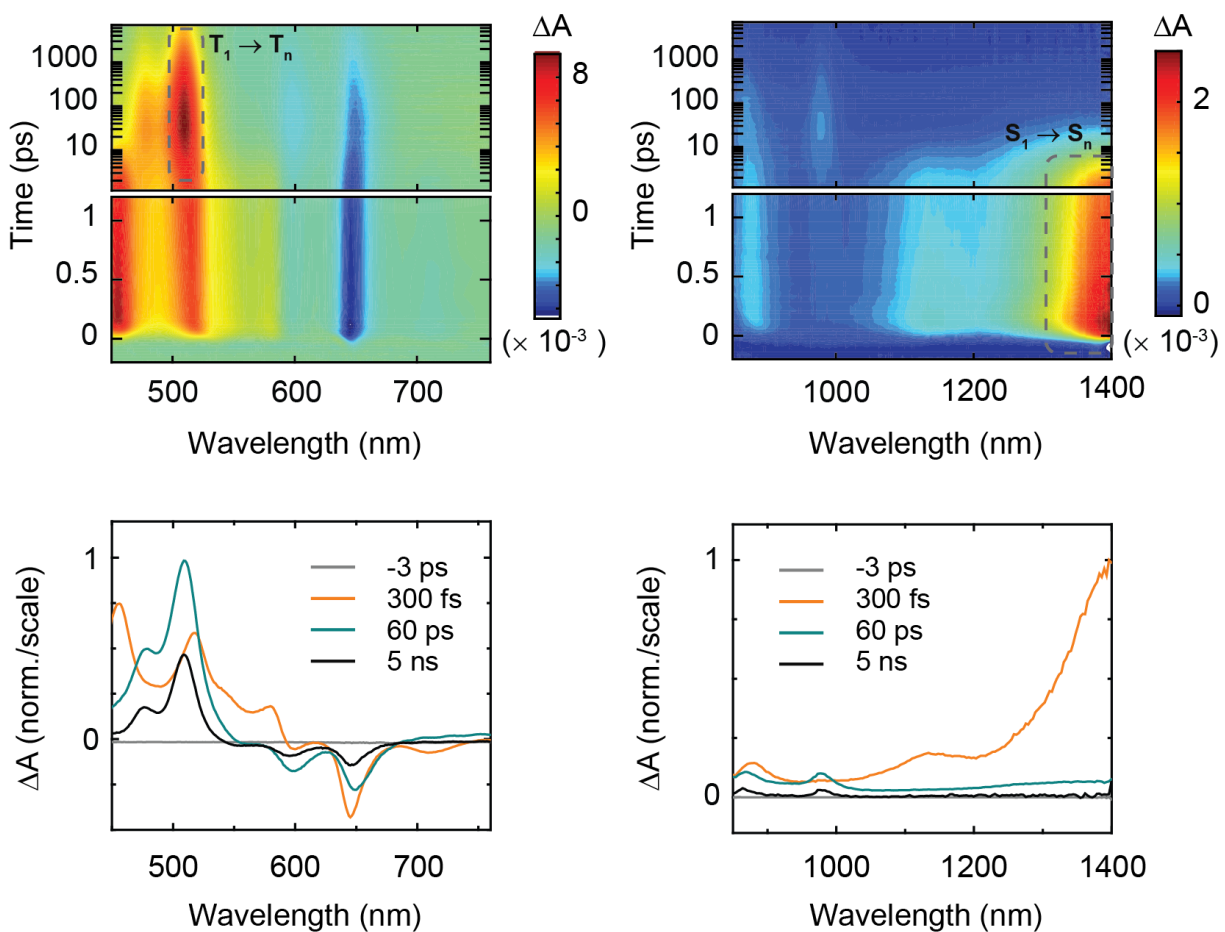


Figure S7: Transient absorption spectrum of an aqueous nanoparticle suspension of TIPS-Pn alkyne **4** at room temperature. A pump wavelength of 647 nm was used. Singlet (S_1 - S_n) and triplet (T_1 - T_n) photoinduced absorption features have been indicated on the visible (panel (a)) and NIR (panel (b)) surface plots. A triplet pair formation time of ~ 7 ps was determined from a single exponential fit to the decay of the parent singlet exciton photoinduced absorption at 450-465 ns.

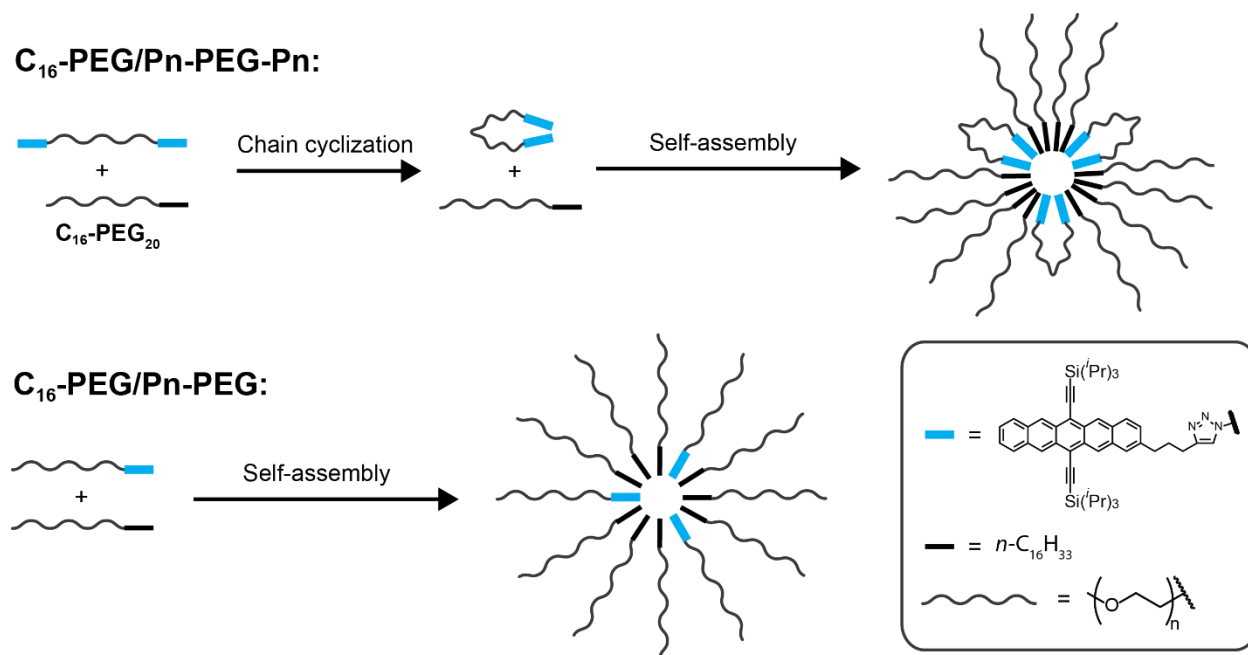


Figure S8: Proposed mechanism of C₁₆-PEG/Pn-PEG-Pn (top panel) and C₁₆-PEG/Pn-PEG (bottom panel) mixed micelles.

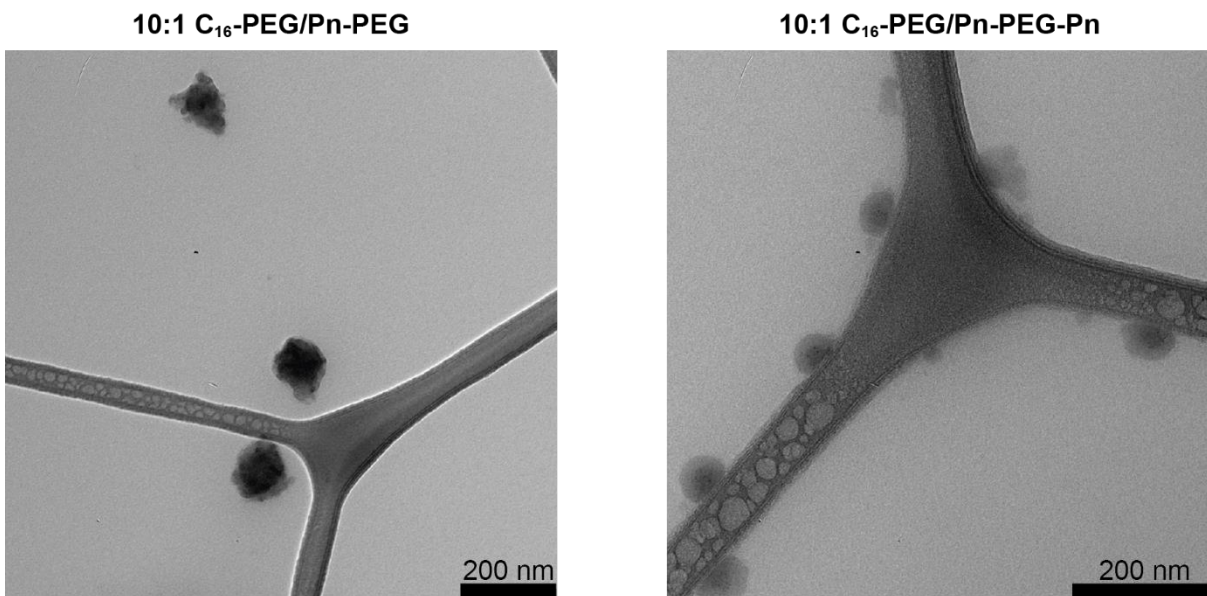


Figure S9: Transmission electron micrographs of 10:1 C₁₆-PEG/Pn-PEG (left panel) and 10:1 C₁₆-PEG/Pn-PEG-Pn mixed micelles imaged on ultrathin carbon film on lacey carbon supports. The micelles tended to associate with the carbon support of the grids.

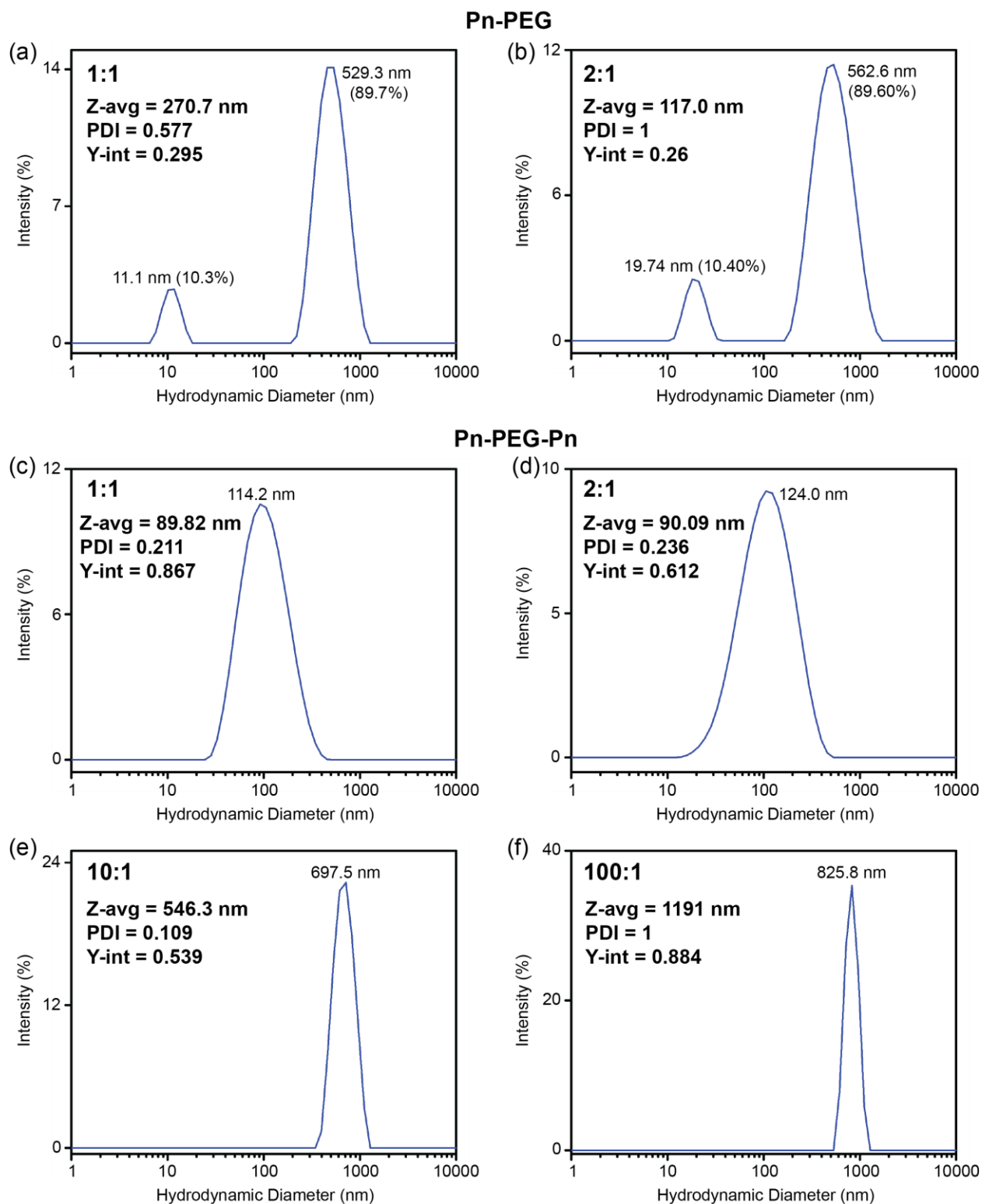


Figure S10: Results of dynamic light scattering experiments on aqueous suspensions of mixed micelles of C₁₆-PEG/Pn-PEG (panels (a) and (b)) and C₁₆-PEG/Pn-PEG-Pn (panels (c)-(f)) at 25 °C. Peak diameters are indicated next to the corresponding peak. In mixed micelles of C₁₆-

PEG/Pn-PEG, the relative contribution of each peak to the total intensity is given in brackets next to the peak diameter. The lower intensity peaks 11.1 and 19.74 nm in the 1:1 and 2:1 suspensions of C₁₆-PEG/Pn-PEG are possibly due to dissociation of Pn-PEG micelles. These peaks being attributed to micelles of C₁₆-PEG is ruled out on the basis that this polymer does not form solution aggregates at the concentrations used to precipitate these mixed micelles (see Figure S12). Dynamic light scattering data on 10:1 and 100:1 mixed micelle suspensions of C₁₆-PEG:Pn-PEG could not be obtained due to significant sample polydispersity. Autocorrelation functions used for extracting particle size are shown in Figure S11.

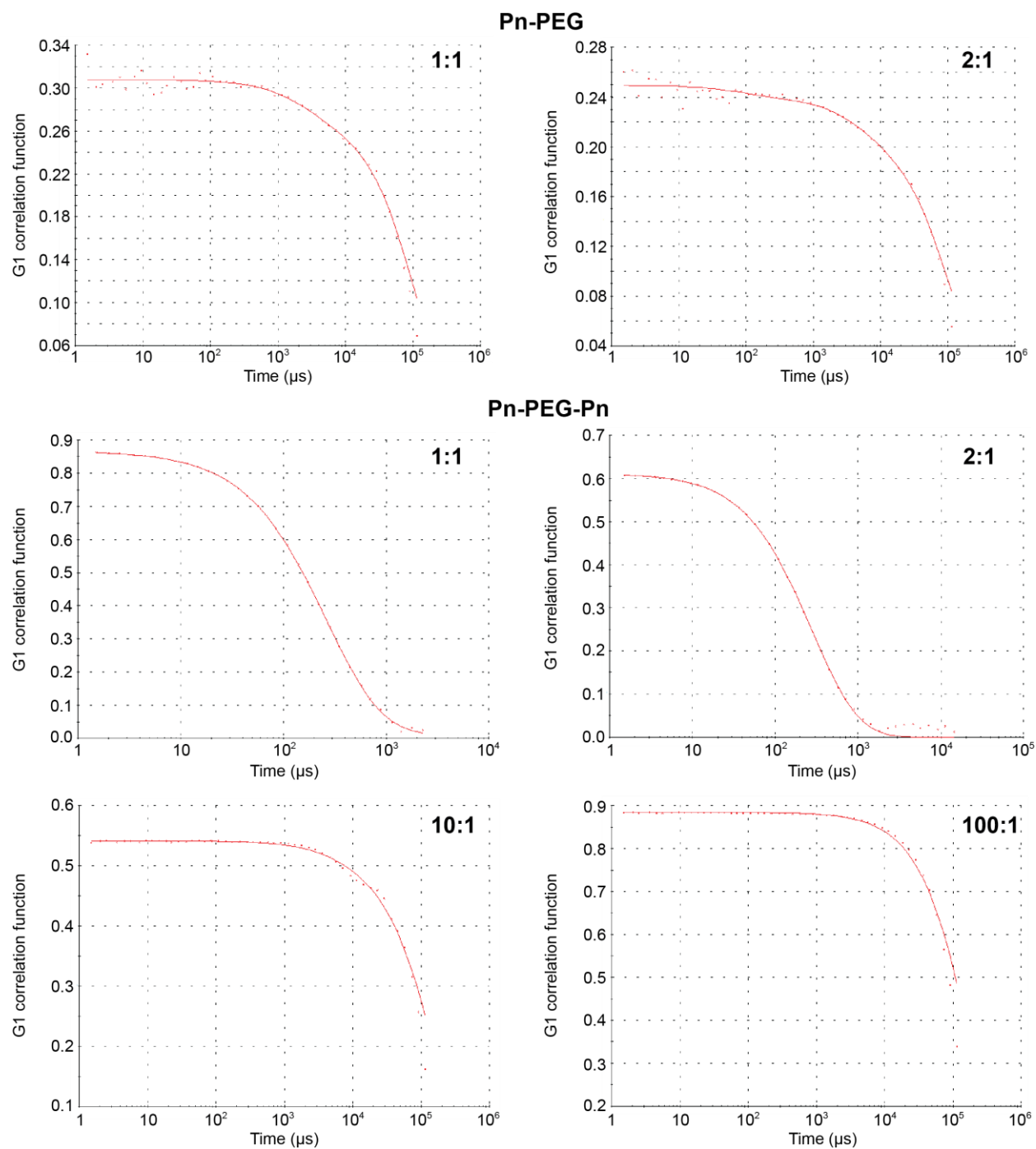


Figure S11: Autocorrelation functions used to extract particle size of mixed micelle suspensions of C₁₆-PEG/Pn-PEG and C₁₆-PEG/Pn-PEG-Pn at various incorporation ratios.

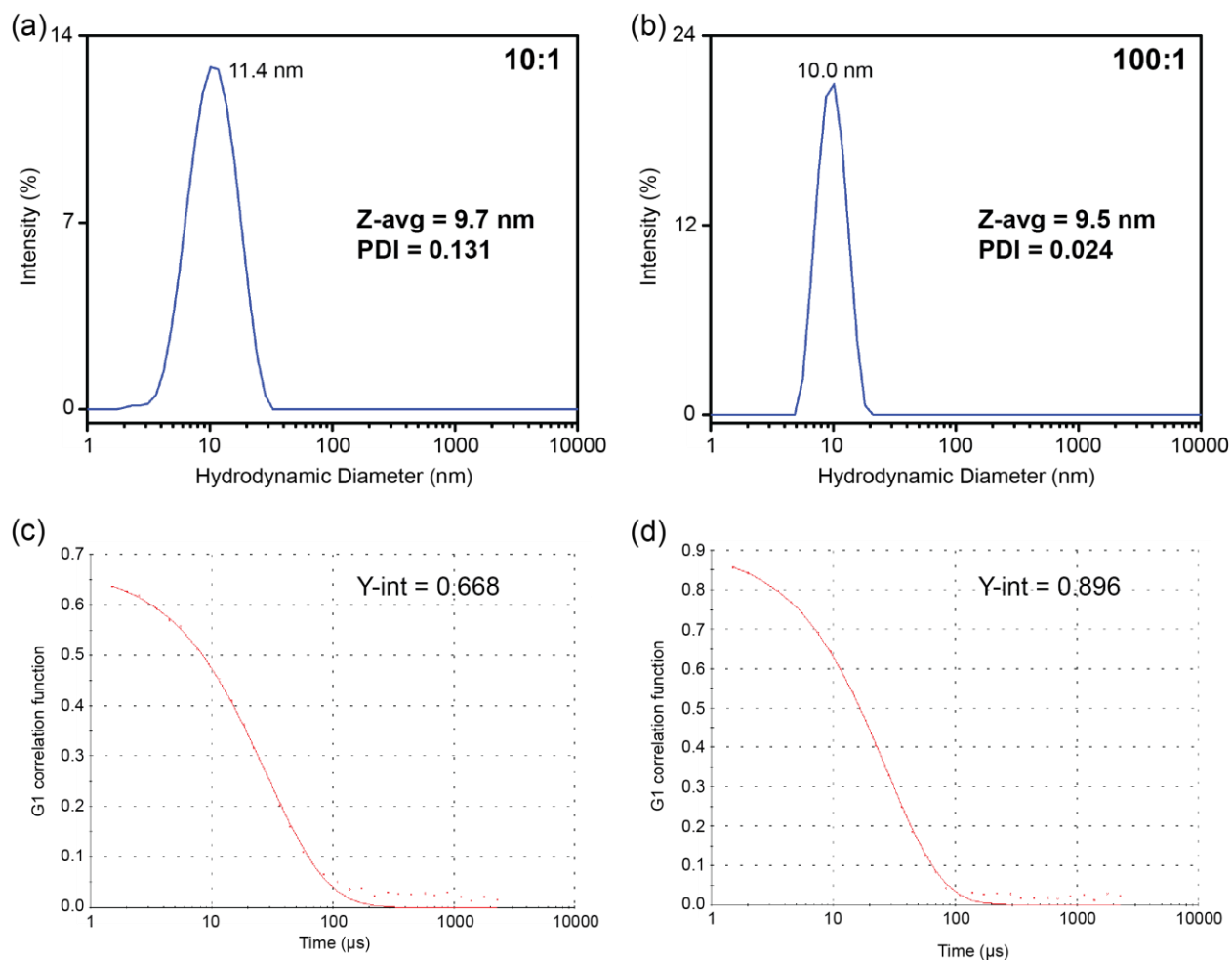


Figure S12: Results of dynamic light scattering experiments on aqueous suspensions of C₁₆-PEG micelles at 25 °C. Size distributions are shown in panels (a) and (b). Panels (c) and (d) show the autocorrelation functions used to extract particle size. Peak diameters are indicated next to the corresponding peak. Dynamic light scattering data could not be recorded at the concentrations required to precipitate 1:1 and 2:1 mixed micelle suspensions due to the absence of solution scatterers (ie a high unimer concentration).

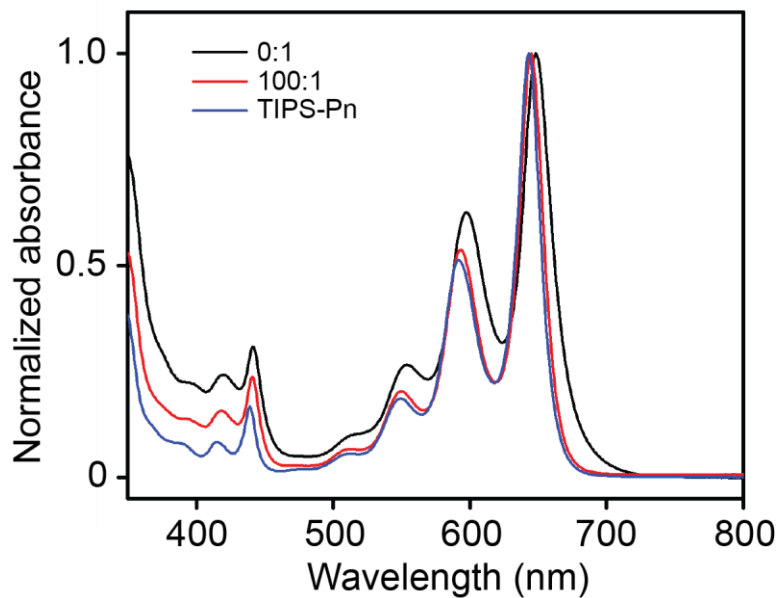


Figure S13: Optical absorption spectra of 0:1 and 100:1 aqueous suspensions of C₁₆-PEG/Pn-PEG mixed micelles. The absorption spectrum of TIPS-Pn in diethylene glycol has been included for comparison. The spectra have been normalized to the peak of the 0-0 vibronic band.

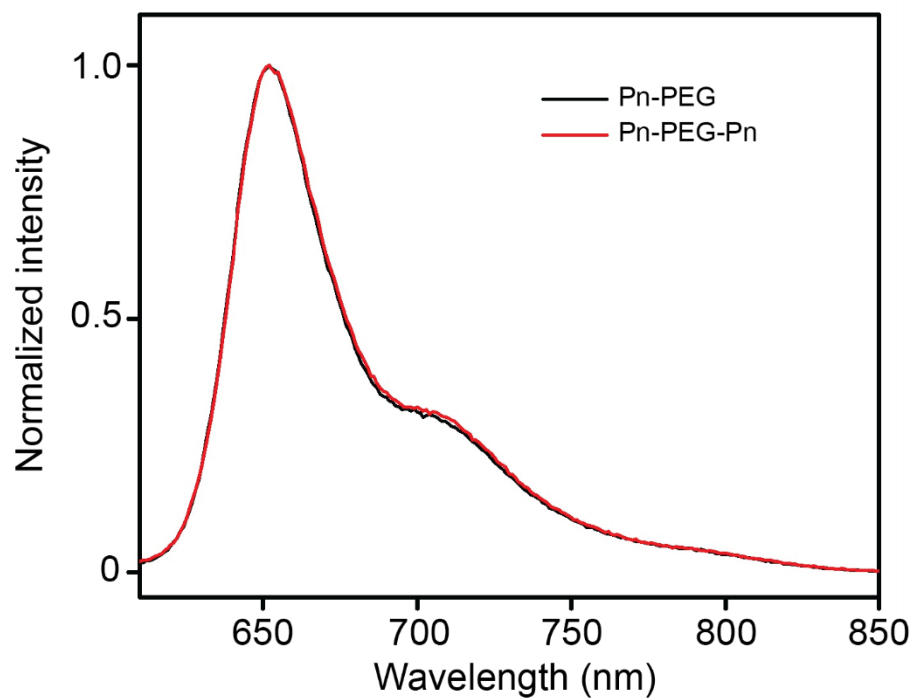


Figure S14: Photoluminescence spectra of Pn-PEG and Pn-PEG-Pn in THF solution. An excitation wavelength of 590 nm was used.

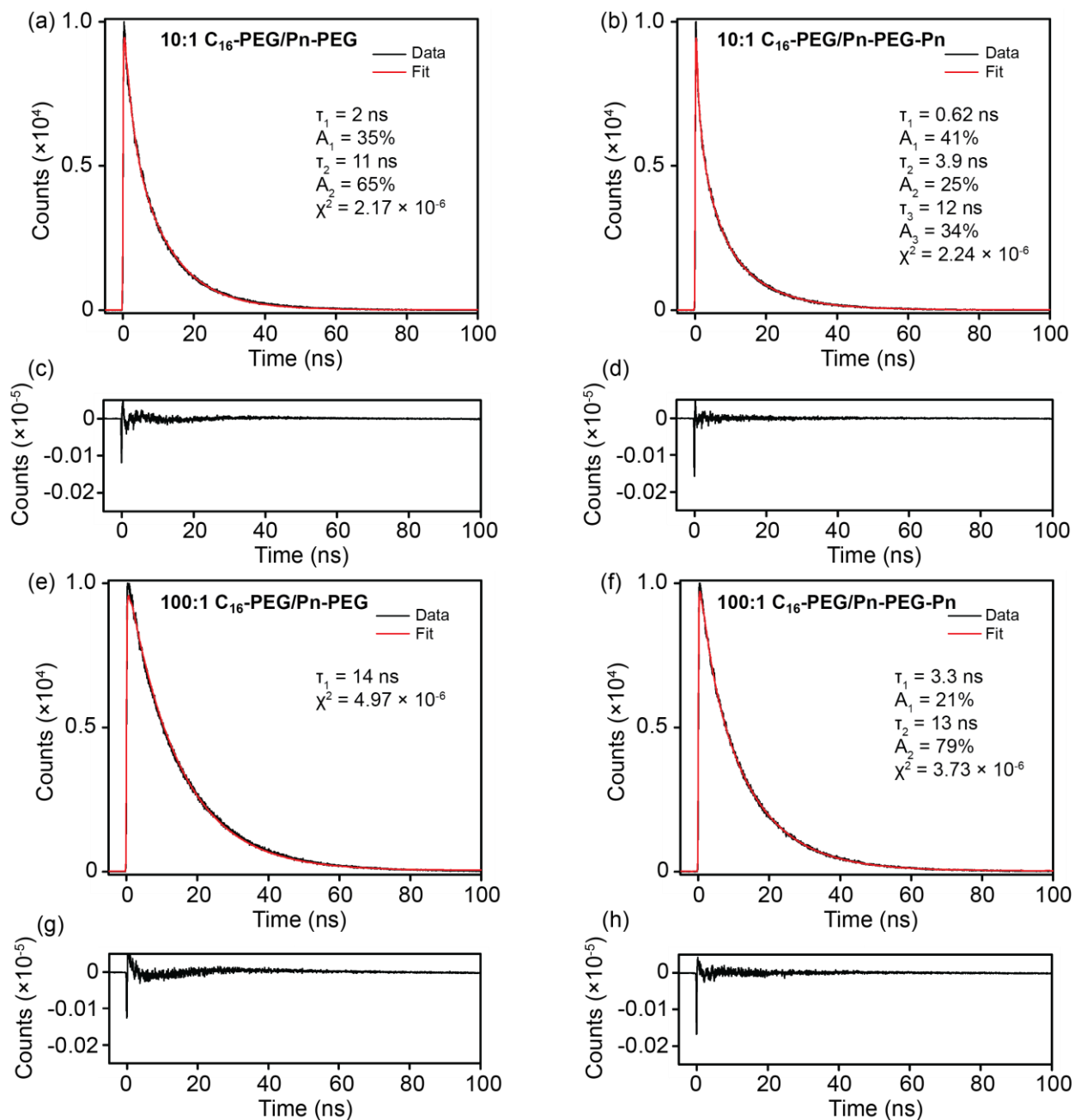


Figure S15: TCSPC traces (panels (a), (b), (e), and (f)) and residuals (panels (c), (d), (g), and (h)) of 10:1 and 100:1 mixed micelle samples. The samples were excited at 570 nm and the emission monitored at 650 nm.

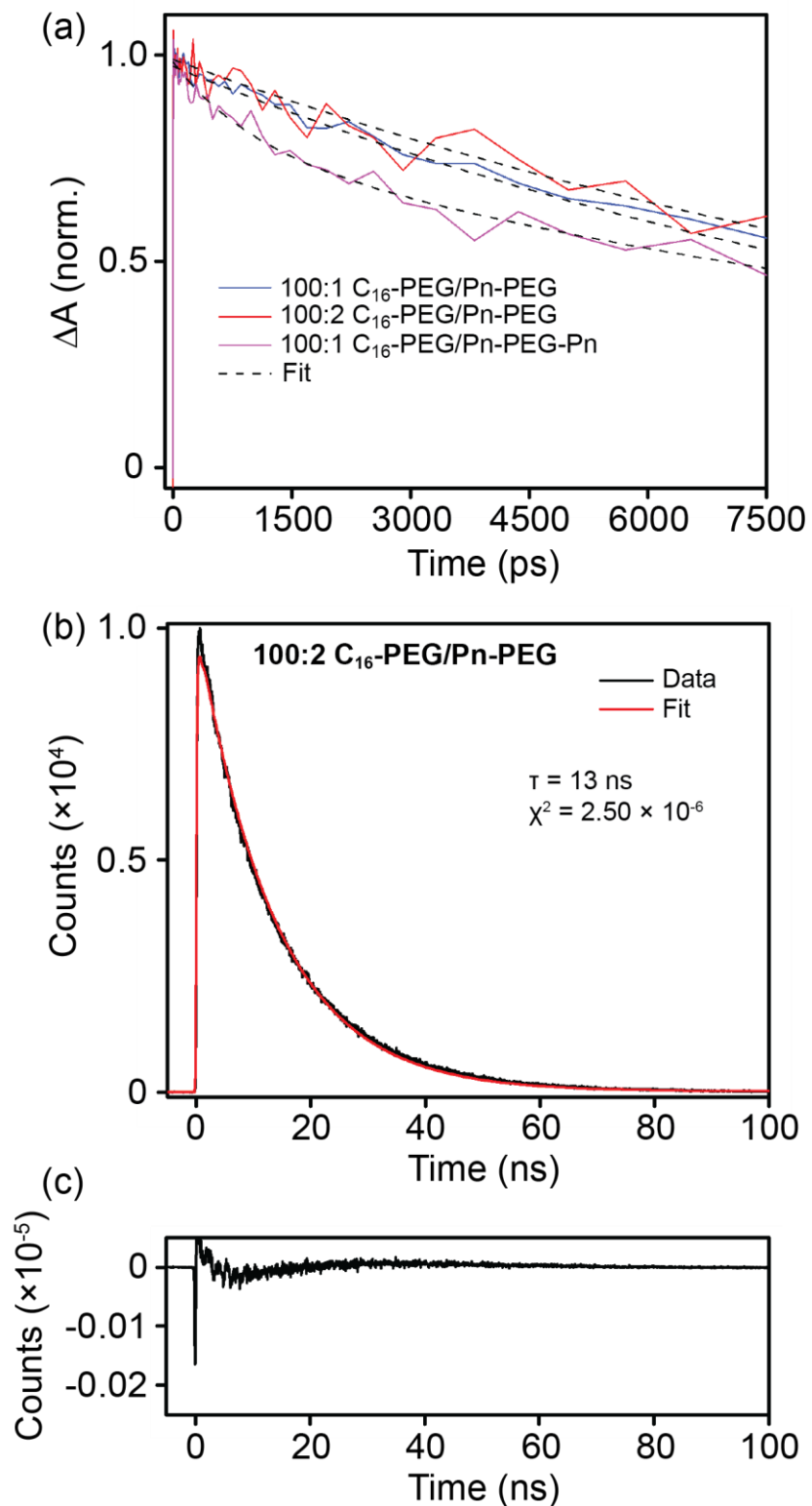


Figure S16: Decay of the parent singlet exciton population in aqueous suspensions of 100:2 C₁₆-PEG/Pn-PEG mixed micelles recorded by transient absorption spectroscopy (panel (a)) and TCSPC (panel (b)). The residuals from a single exponential fit to the TCSPC data are shown in

panel (c). The fluorescence decays were recorded at 650 nm using an excitation wavelength of 570 nm. The decay was modelled using a single exponential function with time constant of 13 ns. The kinetic trace in panel (a) is the decay of the parent singlet photoinduced absorption feature at 445-460 nm. As can be seen in panel (a), parent singlet excitons in 100:2 C₁₆-PEG/Pn-PEG and 100:1 C₁₆-PEG/Pn-PEG show similar decay kinetics. The parent singlet exciton in 100:1 C₁₆-PEG/Pn-PEG-Pn decays shows a clear short-time component, consistent with singlet fission at sites that arise from polymer chain folding.

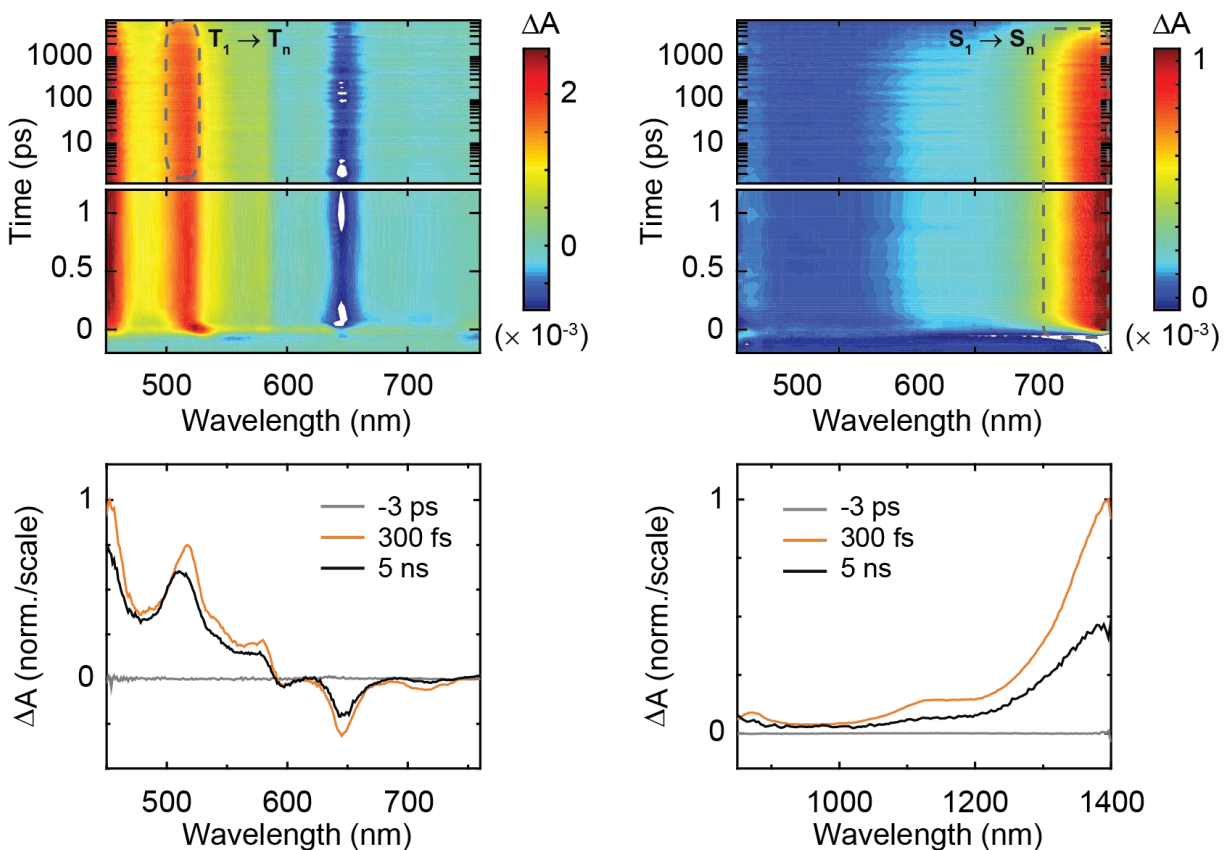


Figure S17: Transient absorption spectrum of an aqueous suspension of 100:2 C₁₆-PEG/Pn-PEG mixed micelles at room temperature. A pump wavelength of 647 nm was used. Singlet (S₁-S_n) and triplet (T₁-T_n) photoinduced absorption features have been indicated on the visible (panel (a)) and NIR (panel (b)) surface plots. A parent singlet exciton lifetime >8000 ps was determined from a single exponential fit to the decay of the parent singlet exciton photoinduced absorption at 450-465 ns (see Figure S16 for the kinetic traces).

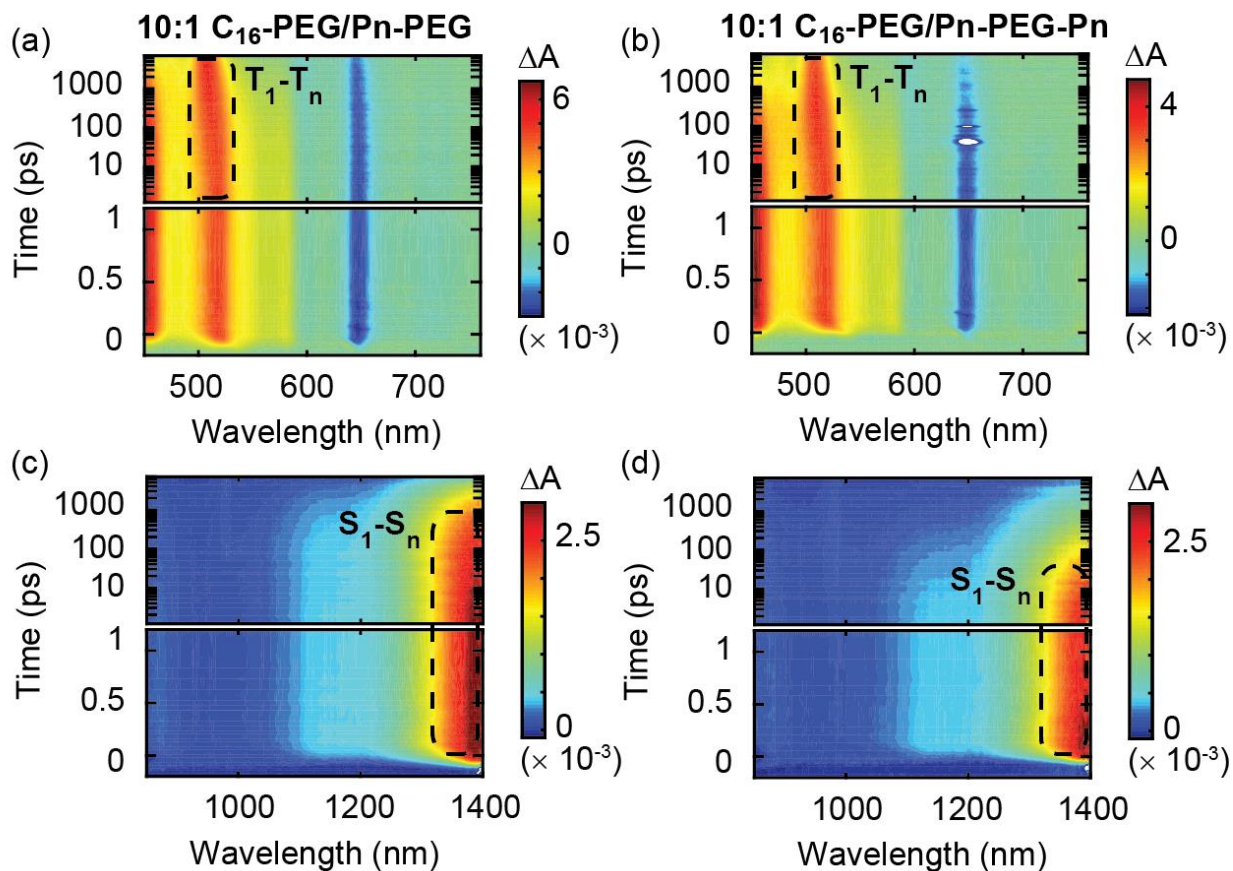
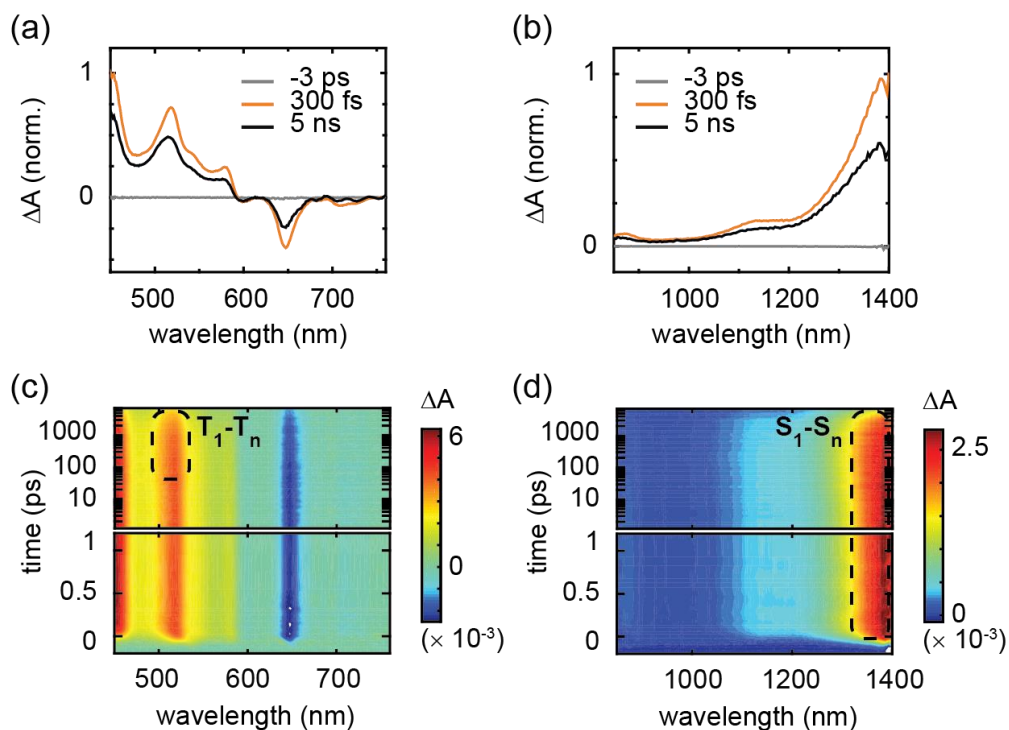


Figure S18: Transient absorption spectra in the visible (panels (a) and (b)) and NIR (panels (c) and (d)) spectral regions of aqueous suspensions of 10:1 mixed micelles. Singlet (S₁-S_n) and triplet (T₁-T_n) photoinduced absorption features have been indicated on the plots. A pump wavelength of 647 nm was used.

100:1 C₁₆-PEG/Pn-PEG



100:1 C₁₆-PEG/Pn-PEG-Pn

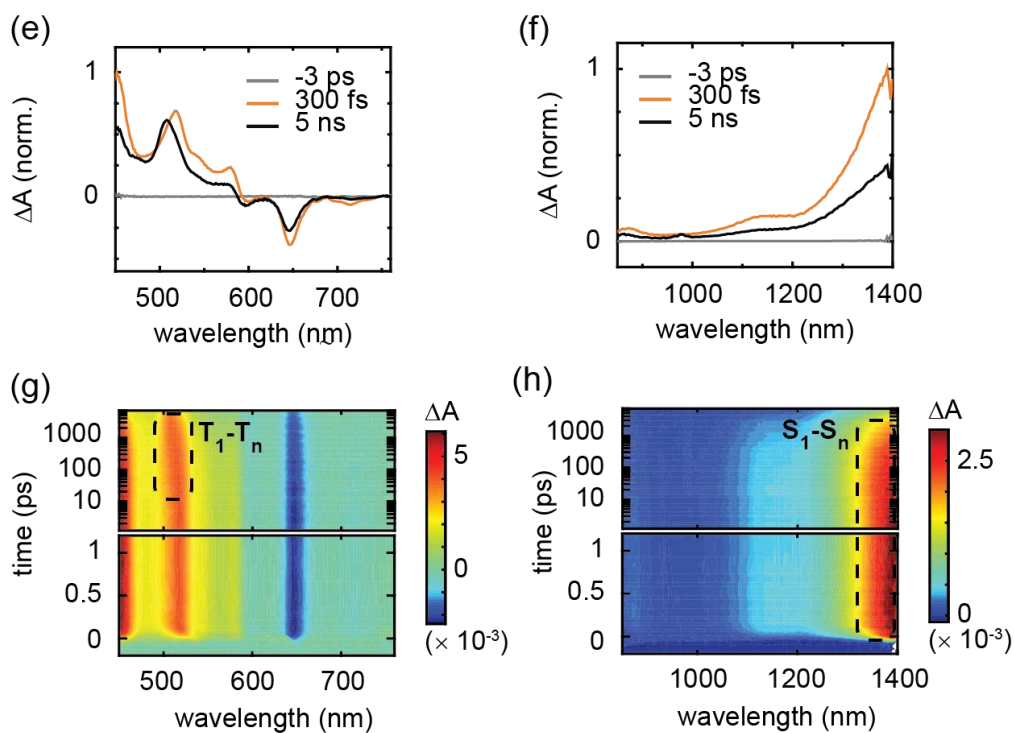


Figure S19: Transient absorption spectra of 100:1 C₁₆-PEG/Pn-PEG and C₁₆-PEG/Pn-PEG-Pn aqueous mixed micelle suspensions in the visible and near-infrared spectral regions. A pump

wavelength of 647 nm was used. The S_1 - S_n near-infrared photoinduced absorption and T_1 - T_n visible photoinduced absorption are indicated on the surface plots in panels (c), (d), (g), and (h).

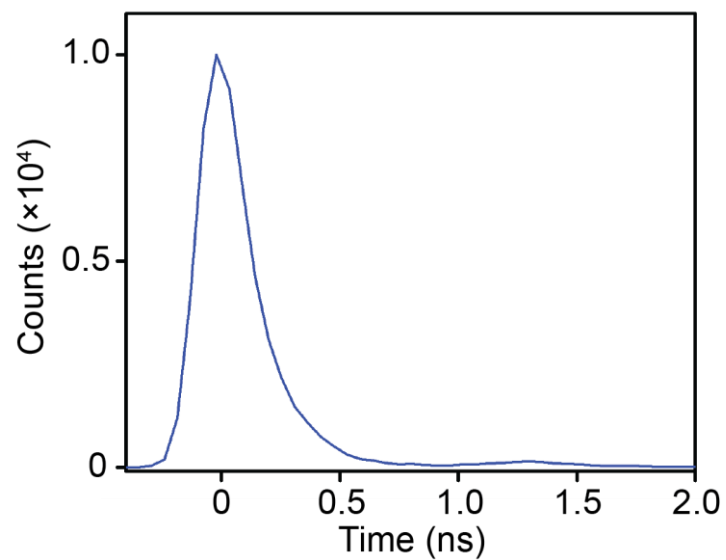


Figure S20: Instrument response function for the TCSPC setup used to record the fluorescence decays. The instrument response is ~200 ps.

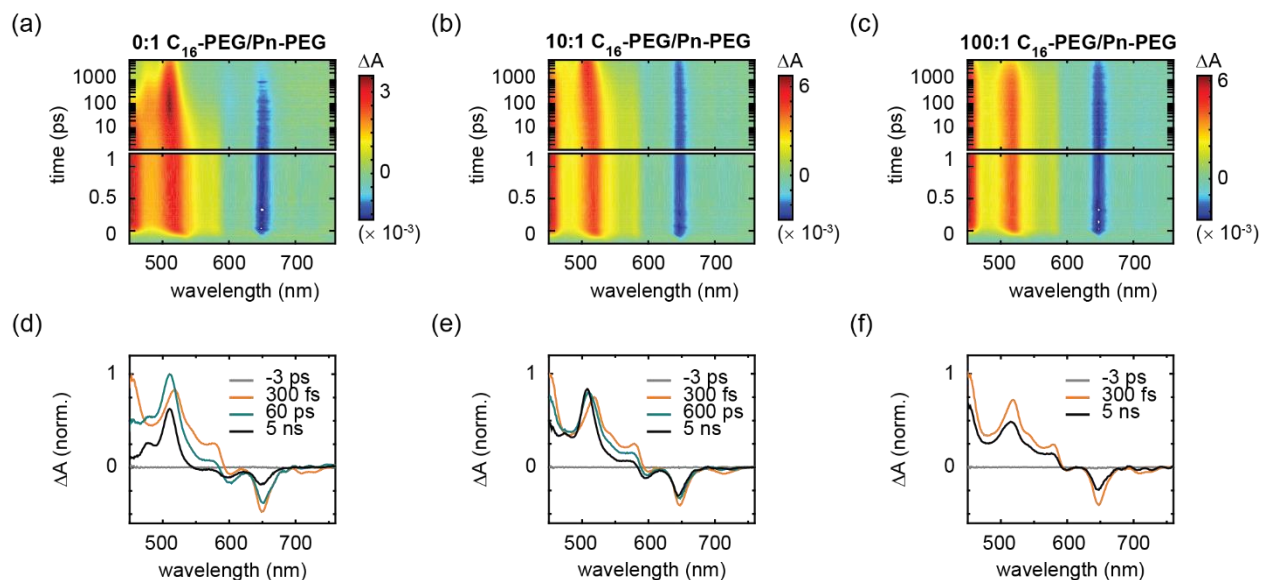


Figure S21: Transient visible absorption of neat and PEG-intercalated Pn-PEG micelles. Surface plots of transient visible absorption of neat and PEG-intercalated Pn-PEG micelles are shown in panels (a) – (c). The experiments were performed with an incident pump wavelength of 647 nm and an incident pump fluence of $130 \mu\text{J cm}^{-2}$. The scale bar is indicated beside each plot. Selected transient spectra for neat and PEG-intercalated Pn-PEG micelles are shown in panels (d) – (f). Spectra time delays are indicated in the legend.

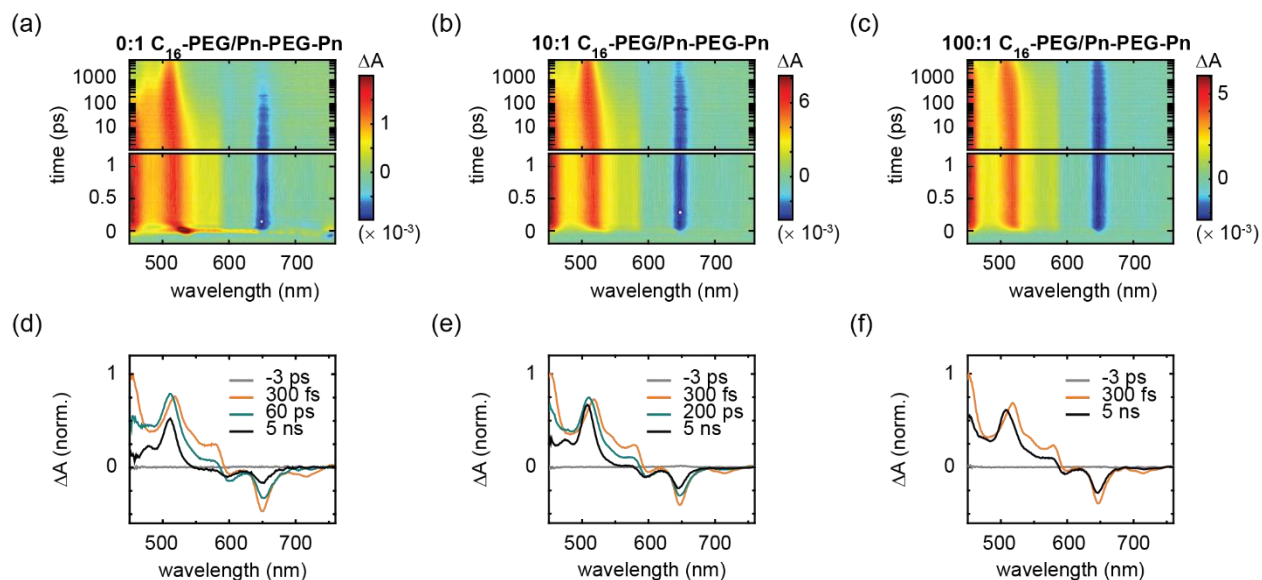


Figure S22: Surface plots of transient visible absorption of neat and PEG-intercalated Pn-PEG-Pn micelles (panels (a) – (c)). The experiments were performed with an incident pump wavelength of 647 nm and an incident pump fluence of 130 and 260 $\mu\text{J cm}^{-2}$ for the 100:1 PEG-Pn-PEG micelles and for the 0:1 and 10:1 PEG-Pn-PEG micelles, respectively. The scale bar is indicated beside each plot. Panels (d) – (f) show selected transient spectra for neat and PEG-intercalated Pn-PEG-Pn micelles. Spectra time delays are indicated in the legend.

Section S4: NMR spectra

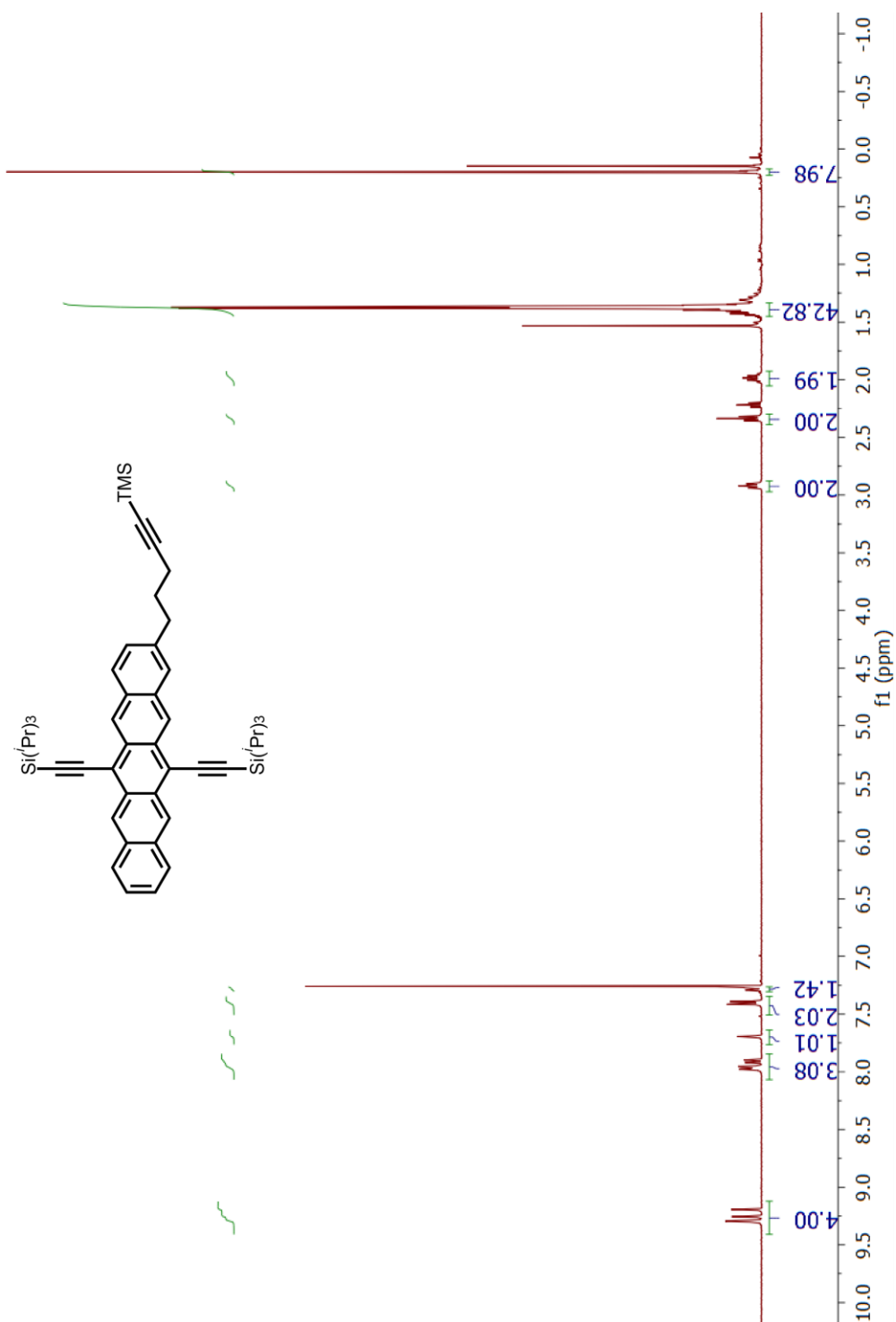


Figure S23: ^1H NMR spectrum of **3** in CDCl_3 .

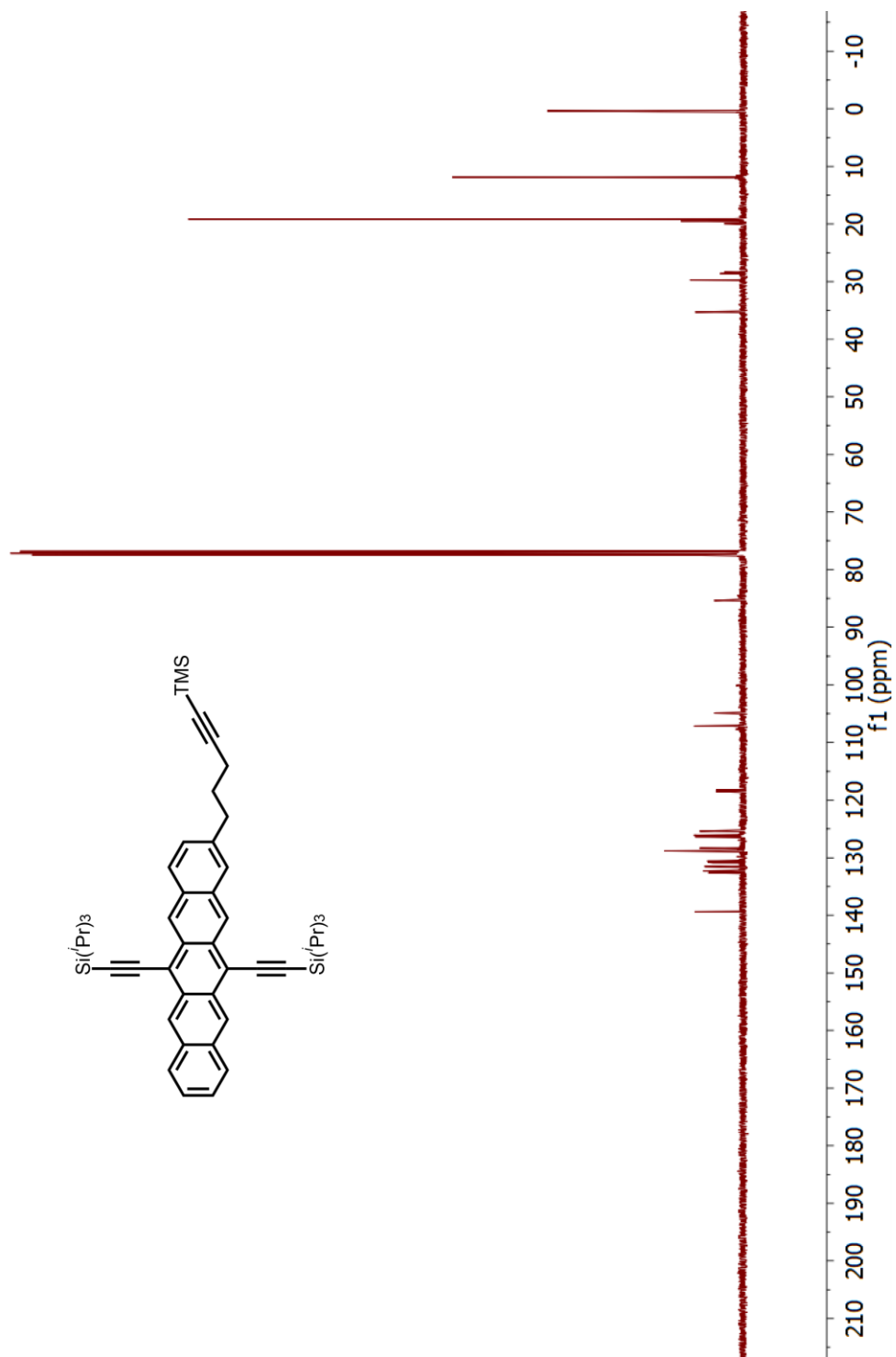


Figure S24: ^{13}C NMR spectrum of **3** in CDCl_3 .

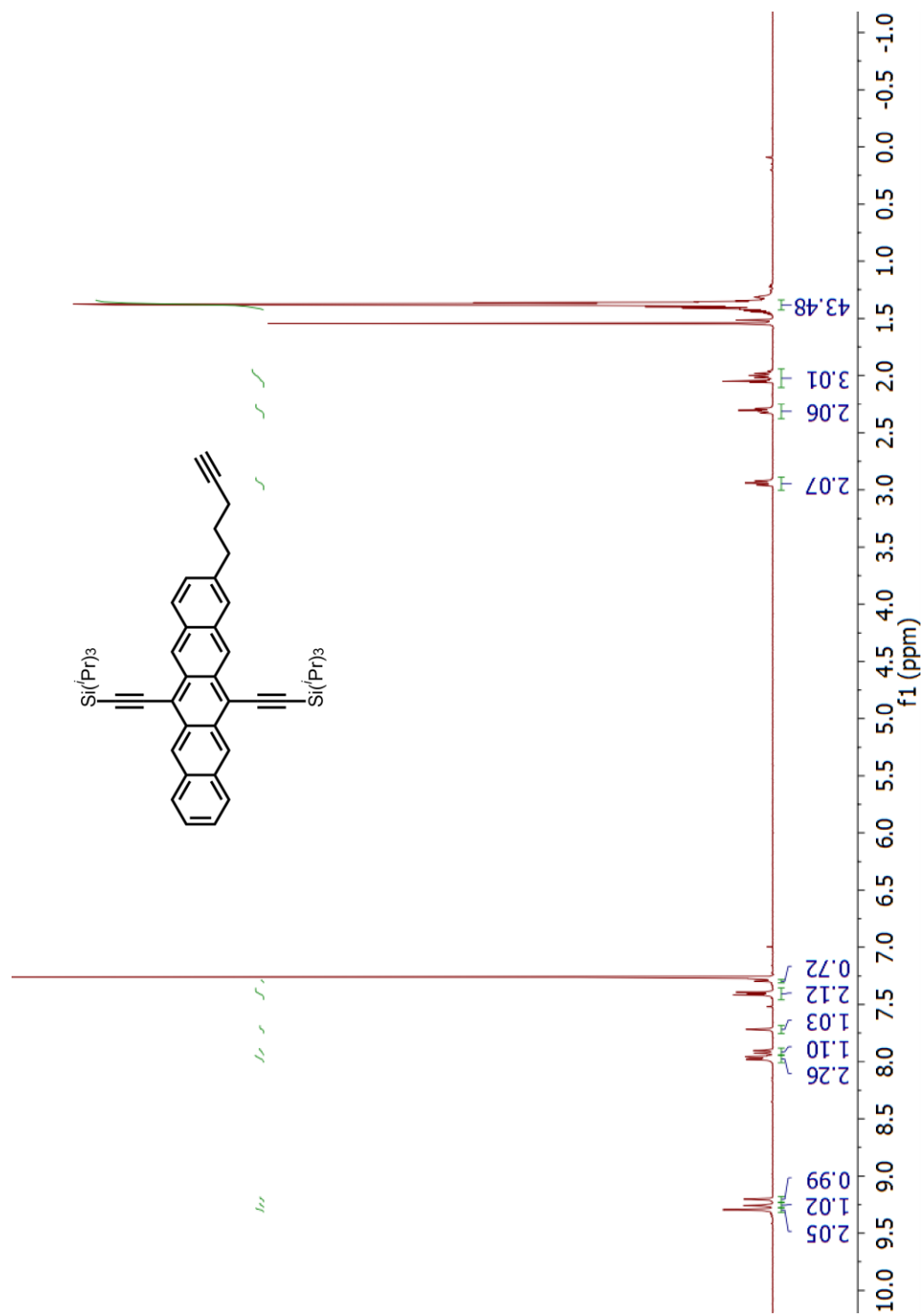


Figure S25: ^1H NMR spectrum of **4** in CDCl_3 .

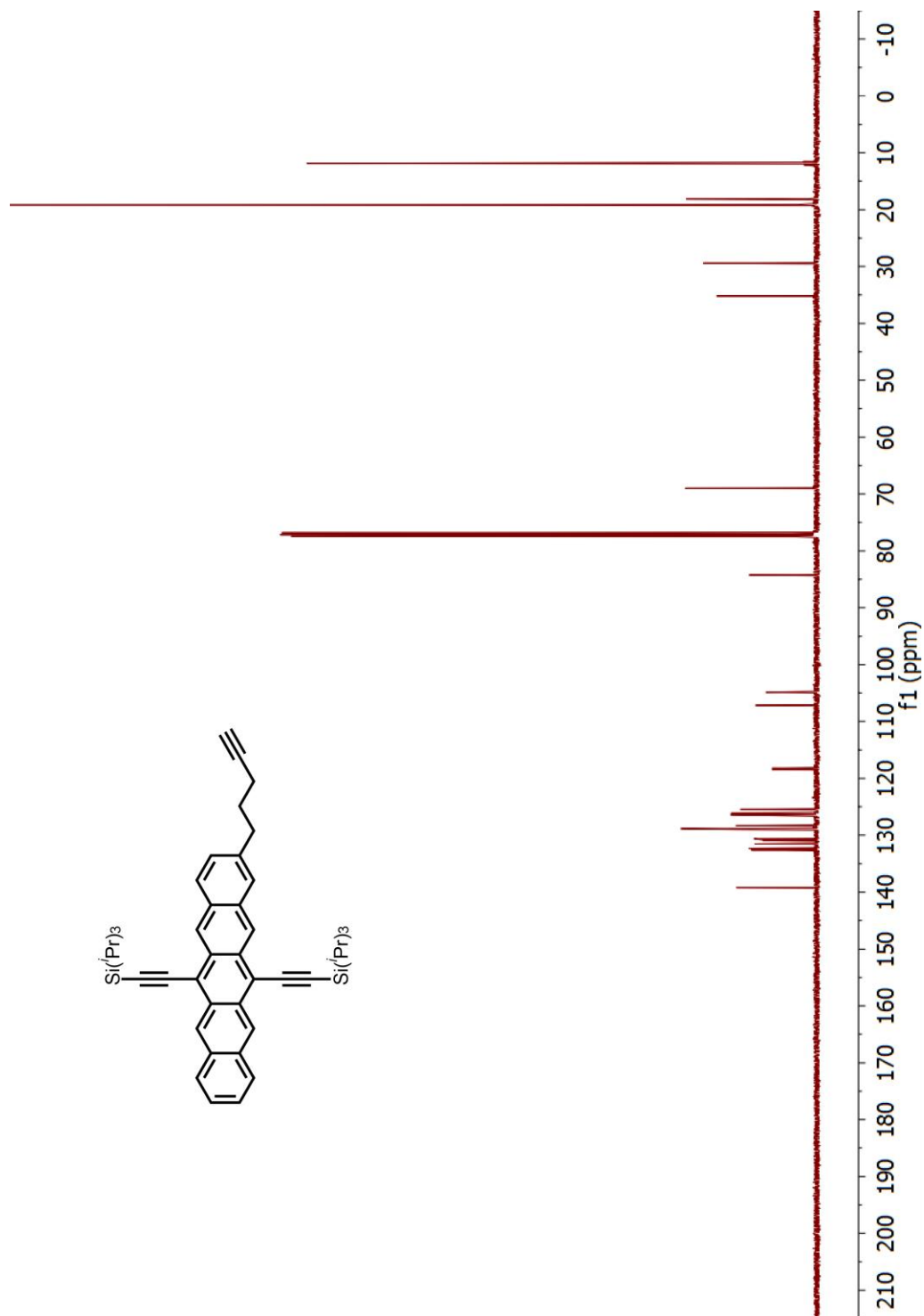


Figure S26: ^{13}C NMR spectrum of **4** in CDCl_3 .

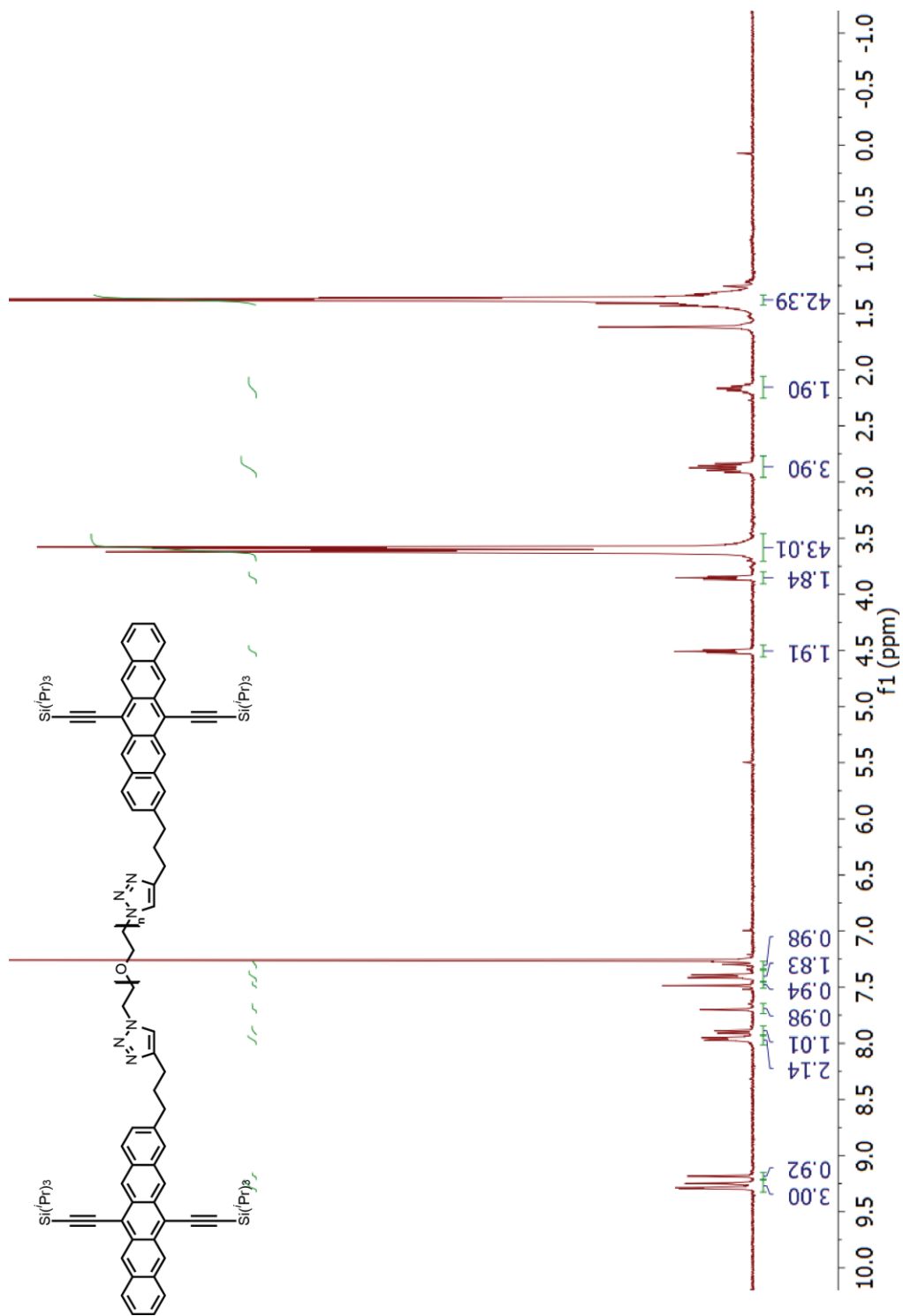


Figure S28: ^1H NMR spectrum of Pn-PEG-Pn in CDCl_3 .

References

- (1) Yao, G.; Steliou, K. Synthetic Studies toward Bioactive Cyclic Peroxides from the Marine Sponge *Plakortis Angulospiculatus*. *Org. Lett.* **2002**, *4*, 485–488.
- (2) Pensack, R. D.; Grieco, C.; Purdum, G. E.; Mazza, S. M.; Tilley, A. J.; Ostroumov, E. E.; Seferos, D. S.; Loo, Y.-L.; Asbury, J. B.; Anthony, J. E.; Scholes, G. D. Solution-Processable, Crystalline Material for Quantitative Singlet Fission. *Mater. Horiz.* **2017**, *4*, 915–923.
- (3) Pensack, R. D.; Ostroumov, E. E.; Tilley, A. J.; Mazza, S.; Grieco, C.; Thorley, K. J.; Asbury, J. B.; Seferos, D. S.; Anthony, J. E.; Scholes, G. D. Observation of Two Triplet-Pair Intermediates in Singlet Exciton Fission. *J. Phys. Chem. Lett.* **2016**, *7*, 2370–2375.
- (4) Hall, P.; Selinger, B. Better Estimates of Exponential Decay Parameters. *J. Phys. Chem.* **1981**, *85*, 2941–2946.
- (5) Sanders, S. N.; Kumarasamy, E.; Pun, A. B.; Trinh, M. T.; Choi, B.; Xia, J.; Taffet, E. J.; Low, J. Z.; Miller, J. R.; Roy, X.; Zhu, X.-Y.; Steigerwald, M. L.; Sfeir, M. Y.; Campos, L. M. Quantitative Intramolecular Singlet Fission in Bipentacenes. *J. Am. Chem. Soc.* **2015**, *137*, 8965–8972.
- (6) Sanders, S. N.; Kumarasamy, E.; Pun, A. B.; Appavoo, K.; Steigerwald, M. L.; Campos, L. M.; Sfeir, M. Y. Exciton Correlations in Intramolecular Singlet Fission. *J. Am. Chem. Soc.* **2016**, *138*, 7289–7297.
- (7) Sanders, S. N.; Kumarasamy, E.; Pun, A. B.; Steigerwald, M. L.; Sfeir, M. Y.; Campos, L. M. Singlet Fission in Polypentacene. *Chem* **2016**, *1*, 505–511.
- (8) Kraft, U.; Anthony, J. E.; Ripaud, E.; Loth, M. A.; Weber, E.; Klauk, H. Low-Voltage Organic Transistors Based on Tetraceno[2,3-b]Thiophene: Contact Resistance and Air Stability. *Chem. Mater.* **2015**, *27*, 998–1004.
- (9) Plunkett, K. N.; Godula, K.; Nuckolls, C.; Tremblay, N.; Whalley, A. C.; Xiao, S. Expedient Synthesis of Contorted Hexabenzocoronenes. *Org. Lett.* **2009**, *11*, 2225–2228.
- (10) Anthony, J. E.; Eaton, D. L.; Parkin, S. R. A Road Map to Stable, Soluble, Easily Crystallized Pentacene Derivatives. *Org. Lett.* **2002**, *4*, 15–18.
- (11) Farinha, J. P. S.; Piçarra, S.; Miesel, K.; Martinho, J. M. G. Fluorescence Study of the Coil-Globule Transition of a PEO Chain in Toluene. *J. Phys. Chem. B* **2001**, *105*, 10536–10545.
- (12) Char, K.; Frank, C. W.; Gast, A. P.; Tang, W. T. Hydrophobic Attraction of Pyrene-End-Labeled Poly(Ethylene Glycol) in Water and Water-Methanol Mixtures. *Macromolecules* **1987**, *20*, 1833–1838.
- (13) Char, K.; Frank, C. W.; Gast, A. P. Consideration of Hydrophobic Attractions in End-to-End Cyclization. *Macromolecules* **1989**, *22*, 3177–3180.

- (14) Israelachvili, J.; Pashley, R. The Hydrophobic Interaction Is Long Range, Decaying Exponentially with Distance. *Nature* **1982**, *300*, 341–342.
- (15) Pensack, R. D.; Tilley, A. J.; Parkin, S. R.; Lee, T. S.; Payne, M. M.; Gao, D.; Jahnke, A. A.; Oblinsky, D. G.; Li, P.-F.; Anthony, J. E.; Seferos, D. S.; Scholes, G. D. Exciton Delocalization Drives Rapid Singlet Fission in Nanoparticles of Acene Derivatives. *J. Am. Chem. Soc.* **2015**, *137*, 6790–6803.
- (16) Pensack, R. D.; Tilley, A. J.; Grieco, C.; Purdum, G. E.; Ostroumov, E. E.; Granger, D. B.; Oblinsky, D. G.; Dean, J. C.; Doucette, G. S.; Asbury, J. B.; Loo, Y.-L.; Seferos, D. S.; Anthony, J. E.; Scholes, G. D. Striking the Right Balance of Intermolecular Coupling for High-Efficiency Singlet Fission. *Chem. Sci.* **2018**, doi:10.1039/C8SC00293B.
- (17) Roberts, S. T.; McAnally, R. E.; Mastron, J. N.; Webber, D. H.; Whited, M. T.; Brutchey, R. L.; Thompson, M. E.; Bradforth, S. E. Efficient Singlet Fission Discovered in a Disordered Acene Film. *J. Am. Chem. Soc.* **2012**, *134*, 6388–6400.
- (18) Walker, B. J.; Musser, A. J.; Beljonne, D.; Friend, R. H. Singlet Exciton Fission in Solution. *Nat. Chem.* **2013**, *5*, 1019–1024.